DOI: 10.1093/jnci/djr360
Advance Access publication on October 24, 2011.

ARTICLE

The Role of Polymeric Immunoglobulin Receptor in Inflammation-Induced Tumor Metastasis of Human Hepatocellular Carcinoma

Jing Ai, Qingjuan Tang, Yanlin Wu, Yang Xu, Teng Feng, Ruiyu Zhou, Yi Chen, Xin Gao, Qingfeng Zhu, Xihua Yue, Qiuming Pan, Siyun Xu, Jing Li, Min Huang, Jennifer Daugherty-Holtrop, Yuanzheng He, H. Eric Xu, Jia Fan, Jian Ding, Meiyu Geng

Manuscript received April 18, 2011; revised August 16, 2011; accepted August 17, 2011.

Correspondence to: Meiyu Geng, PhD and Jian Ding, MD, PhD, Division of Anti-tumor Pharmacology, State Key Laboratory of Drug Research, Shanghai Institute of Materia Medica, Chinese Academy of Sciences, 555 Zuchongzhi Rd, Shanghai 201203, People's Republic of China (e-mail: mygeng@mail.shcnc.ac.cn; suozhang@mail.shcnc.ac.cn) and Jia Fan, MD, Department of Liver Surgery, Liver Cancer Institute, Zhongshan Hospital and Shanghai Medical School, and Institute of Biomedical Sciences, Fudan University, 180 Fenglin Rd, Shanghai 200032, People's Republic of China (e-mail: jiafan99@yahoo.com).

Background Expression of the polymeric immunoglobulin receptor (pIgR), a transporter of polymeric IgA and IgM, is commonly increased in response to viral or bacterial infections, linking innate and adaptive immunity. Abnormal expression of pIgR in cancer was also observed, but its clinical relevance remains uncertain.

Methods A human hepatocellular carcinoma (HCC) tissue microarray (n = 254) was used to investigate the association between pIgR expression and early recurrence. An experimental lung metastasis model using severe combined immune-deficient mice was applied to determine the metastatic potential of Madin–Darby canine kidney (n = 5 mice per group) and SMMC-7721 (n = 12 mice per group) cells overexpressing pIgR vs control cells. RNA interference, immunoprecipitation, and immunoblotting were performed to investigate the potential role for pIgR in the induction of epithelial–mesenchymal transition (EMT). In vitro studies (co-immunoprecipitation, immunoblotting, and migration, invasion, and adhesion assays) were used to determine the mechanisms behind pIgR-mediated metastasis. All statistical tests were two-sided.

Results High expression of pIgR was statistically significantly associated with early recurrence in early-stage HCC and in hepatitis B surface antigen–positive HCC patients (log-rank $P = .02$). Mice injected with pIgR-overexpressing cells had a statistically significantly higher number of lung metastases compared with respective control cells (Madin–Darby canine kidney cells: pIgR mean = 29.4 metastatic nodules per lung vs control mean = 0.0 metastatic nodules per lung, difference = 29.4 metastatic nodules per lung, 95% confidence interval = 13.0 to 45.8, $P = .001$; SMMC-7721 cells: pIgR mean = 10.4 metastatic nodules per lung vs control mean = 2.2 metastatic nodules per lung, difference = 8.2 metastatic nodules per lung, 95% confidence interval = 1.0 to 15.5, $P = .03$). Furthermore, high expression of pIgR was sufficient to induce EMT through activation of Smad signaling.

Conclusions pIgR plays a role in the induction of EMT. Our results identify pIgR as a potential link between hepatitis B virus–derived hepatitis and HCC metastasis and provide evidence in support of pIgR as a prognostic biomarker for HCC and a potential therapeutic target.

J Natl Cancer Inst 2011;103:1696–1712

Hepatocellular carcinoma (HCC) is the third leading cause of cancer-induced death worldwide, and patients have a very poor prognosis (1–3). Surgical resection, in the form of partial hepatectomy or liver transplantation, is the mainstay of curative treatment. Nonetheless, recurrence of HCC is still common after curative surgery. In addition, HCC is frequently diagnosed at an advanced stage and thus precludes curative treatment. No effective therapeutic option exists for the treatment of the majority of patients with liver cancer (4–8). Etiologically, HCC commonly occurs in patients with chronic hepatitis, resulting from inflammation in response to hepatitis B virus (HBV) or hepatitis C virus (HCV) infections. In fact, more than half of all HCCs in the world are attributed to chronic hepatitis B (1–3,9). Although this link has been recognized for decades, the molecular mechanisms of how chronic hepatitis promotes HCC tumorigenesis and metastasis remain largely unclear.

The epithelial–mesenchymal transition (EMT), in which epithelial cancer cells lose their polarity and become motile mesenchymal cells, has been implicated in cancer invasion and metastasis (10). Cancer cells undergoing EMT appear to exhibit properties of cancer stem cells (11), override oncogene-induced premature senescence and apoptosis (12), and contribute to immunosuppression

(13), indicating the vital role of EMT in tumor recurrence. Recent advances in understanding cancer progression point to EMT as a key event linking inflammation with cancer metastasis (14). As EMT appears to play a pivotal role in hepatocellular dissemination during HCC progression (15), probing insights into the molecular mechanisms of how EMT links chronic hepatitis and HCC progression may benefit the pathological assessments and therapeutic options for these patients.

The polymeric immunoglobulin receptor (pIgR) is a transporter of dimeric IgA (dIgA) and pentameric IgM (pIgM), which are the first-line antibodies in response to initial infection. Widely expressed in epithelial cells, pIgR expression is also commonly increased by proinflammatory cytokines in response to viral or bacterial infections, thus linking innate and adaptive immunity (16–19). Abnormal expression of pIgR in malignantly transformed epithelial cells was initially reported 30 years ago (20–23). High levels of the cleaved extracellular domain of pIgR, designated as the secretory component, were also detected in the sera of patients with HCC and colonic carcinoma with liver metastasis (24). However, the clinical relevance and potential function of pIgR in tumor cells remain uncertain.

In this study, we investigated the relationship between pIgR expression and clinical outcome (overall survival, recurrence and disease-free survival [DFS]) in 254 HCC patients enrolled in a Chinese study. The potential role for pIgR in EMT was investigated in patient samples and HCC cell lines by immunohistochemistry (IHC), co-immunoprecipitation, immunoblotting, and migration, invasion, and adhesion assays. Furthermore, we studied the metastatic potential of pIgR-overexpressing cells in an experimental lung metastasis mouse model.

CONTEXT AND CAVEATS

Prior knowledge

Although hepatocellular carcinoma (HCC) has been linked to chronic hepatitis B, the underlying molecular mechanisms behind tumorigenesis and metastasis in chronic hepatitis B patients are unclear.

Study design

The polymeric immunoglobulin receptor (pIgR) transports immunoglobulins, and its expression is increased in response to proinflammatory cytokines as part of the adaptive immune response. Abnormal expression of pIgR has been previously reported in HCC patients. This study investigated the relationship between pIgR expression and clinical outcome in 254 HCC patients. In vitro and in vivo experiments with human HCC cell lines were done to determine the role of pIgR in epithelial–mesenchymal transition.

Contribution

High expression of pIgR was associated with early recurrence in patients with early-stage disease and in those who were positive for hepatitis B. Overexpression of pIgR resulted in increased lung metastases in an experimental lung metastases model. In vitro experiments show that overexpression of pIgR induces epithelial–mesenchymal transition in HCC cells, which is regulated through the activation of Smad signaling.

Implications

pIgR-mediated epithelial–mesenchymal transition is a potential underlying biological mechanism behind the development of HCC and metastases in chronic hepatitis B patients. pIgR may also be a prognostic biomarker and potential therapeutic target for HCC.

Limitations

The pathway involved in the development and progression of HCC in hepatitis B patients may be more complex and include multiple converging pathways that regulate epithelial–mesenchymal transition. Further studies to determine the cause of abnormal pIgR expression and potential therapeutic strategies are needed.

From the Editors

Materials and Methods

Clinical Specimens and Analysis of pIgR Expression

Tumor specimens were randomly collected from 254 HCC patients during curative resection from February 15, 2004, to December 15, 2005, in the Liver Cancer Institute, Zhong Shan Hospital, Shanghai, China. The entrance criteria and postsurgical patient surveillance were similar to those specified in previous reports (25,26). Briefly, the enrollment criteria for all patients in this study were 1) definitive HCC diagnosis by pathology on the basis of the World Health Organization criteria; 2) no prior anticancer treatment; 3) surgical resection, defined as complete resection of all tumor nodules with the cut surface being free of cancer by histological examination; 4) availability of suitable formalin-fixed paraffin-embedded tissues and frozen tissues; and 5) availability of complete clinicopathologic and follow-up data. Tumor differentiation was defined according to the Edmondson grading system (27), and liver function was assessed by Child–Pugh classification (28). Tumor staging was defined according to the Sixth Edition of American Joint Committee on Cancer TNM staging manual (29). Patients were re-assessed every 2 months in the first postoperative year and at least every 3–4 months afterward. Follow-up was terminated on May 3, 2010. Most patients died of intrahepatic recurrence, distal metastasis, or complicated liver cirrhosis. All patients were monitored prospectively by serum α-fetoprotein measurement, abdomen ultrasonography, and chest x-ray every 1–6 months, according to the postoperative time. For patients with test results suggestive of recurrence, computed tomography and/or magnetic resonance imaging were used to verify whether intrahepatic recurrence and/or distal metastasis had occurred. The diagnosis of recurrence was made on the basis of typical imaging appearance in computed tomography and/or magnetic resonance imaging scan and an elevated α-fetoprotein level. Patients with confirmed recurrence received further treatments, which followed the same protocol on the basis of tumor size, site, number of tumor nodules, and liver function. Briefly, if the recurrent tumor was localized, a second liver resection, radiofrequency ablation, or percutaneous ethanol injection was suggested. If the recurrent tumor was multiple or diffused, transcatheter arterial chemoembolization was recommended. External radiotherapy was given if lymph node or bone metastases were found; otherwise, symptomatic treatment was provided.

Overall survival was defined as the interval between surgery and either death or the last observation taken. Data were censored at the last follow-up period for living patients. DFS was measured from the date of resection until either detection of recurrent tumor or the last follow-up assessment. In the DFS analysis, data were

censored for patients without tumor recurrence, which represented the occurrence of metastases or de novo tumors and were grouped as early (≤2 years) or late (>2 years) recurrence (30–33). For patients who had a confirmed tumor recurrence, DFS was calculated as the time that early recurrence was first suspected (34,35). Kaplan–Meier survival analysis of male and female patients with high or low pIgR expression was performed, and *P* values were calculated using a two-sided log-rank test. Ethical approval for the use of human subjects was obtained from the Research Ethics Committee of Zhong Shan Hospital. All patients provided written informed consent.

Expression of pIgR and E-cadherin was analyzed via IHC using tissue microarrays, which were constructed as described previously (25,26). Briefly, two core biopsies 1 mm in diameter were obtained from the donor blocks and transferred to the recipient paraffin block at defined array positions. Four different tissue microarray blocks, including tumor and peritumor tissue specimens, were constructed. IHC for pIgR and E-cadherin was performed with monoclonal rabbit anti-human pIgR antibody (dilution, 1:100) or monoclonal mouse anti-human E-cadherin antibody (dilution, 1:600) following a two-step protocol (Novolink Polymer Detection System; Novocastra, Newcastle, UK). IHC staining was assessed by two independent pathologists with no prior knowledge of patient characteristics (Bo Yang and Yuan Ji, Department of Pathology, Zhongshan Hospital, Fudan University, Shanghai, China). Discrepancies were resolved by consensus. The staining extent score was on a scale of 0–4, corresponding to the percentage of immunoreactive tumor cells (0%, 1%–5%, 6%–25%, 26%–75%, and 76%–100%, respectively). The staining intensity was scored as negative (score = 0), weak (score = 1), or strong (score = 2). A score ranging from 0–8 was calculated by multiplying the staining extent score with the intensity score, resulting in a low (0–4) or a high (6–8) expression value for each specimen (36).

Cell Culture

The Madin–Darby canine kidney (MDCK) and human colon adenocarcinoma HT29 cell lines were purchased from the American Type Culture Collection (Manassas, VA). The hepatic carcinoma cell line SMMC-7721 was obtained from the Institute of Biochemistry and Cell Biology, Chinese Academy of Sciences (Shanghai, China). Cells were cultured according to the suppliers' instructions. Briefly, MDCK cells were grown in Delbecco's modified Eagle medium (DMEM; Invitrogen, Grand Island, NY) supplemented with 10% fetal bovine serum (FBS; Invitrogen). HT29 cells were grown in McCoy's 5A medium (Invitrogen) supplemented with 10% FBS. SMMC-7721 cells was cultured in RPMI-1640 medium (Invitrogen) supplemented with 10% FBS (Hangzhou Sijiqing Biological Engineering Materials Co, Ltd, Hangzhou, China). The Phoenix Retroviral Expression System was obtained from American Type Culture Collection (distributed by LGC standards, Middlesex, UK) and grown in DMEM supplemented with 10% FBS. All cell lines were authenticated by using short tandem repeat analysis in July 2009.

Monoclonal and Polyclonal Antibodies

The monoclonal mouse anti-human E-cadherin antibody and the monoclonal mouse anti-human EEA1 antibody were purchased from BD Biosciences (San Diego, CA). The monoclonal rabbit anti-human Smad2 antibody, the polyclonal rabbit anti-human phospho-Smad2 (Ser465/467) antibody, the monoclonal rabbit anti-human Smad3 antibody, the monoclonal rabbit anti-human phospho-Smad3 (Ser423/425) antibody, the monoclonal mouse anti-human Snail antibody, and the monoclonal mouse anti-human Slug antibody were purchased from Cell Signaling Technology (Danvers, MA). The monoclonal mouse anti-human vimentin antibody and the monoclonal mouse anti-human fibronectin antibody were purchased from Abcam (Cambridge, UK). The polyclonal rabbit anti-human pIgR (H300), polyclonal goat anti-human pIgR (N16), polyclonal goat anti-human pIgR (C20), polyclonal rabbit anti-Smad4, normal rabbit IgG, and normal goat IgG antibodies were purchased from Santa Cruz Biotechnology (Santa Cruz, CA). The monoclonal mouse anti-human pan-cytokeratin antibody, polyclonal rabbit anti-human β-actin antibody, monoclonal mouse anti-human TWIST1 antibody, monoclonal mouse anti-human TWIST2 antibody, and polyclonal rabbit anti-human ZEB1 antibody were purchased from Sigma-Aldrich (St Louis, MO). The monoclonal mouse anti-human glyceraldehyde-3-phosphate dehydrogenase (GAPDH) antibody, horseradish peroxidase–conjugated anti-mouse, anti-goat, and anti-rabbit secondary antibodies were all purchased from KangChen Bio-tech (Shanghai, China). Alexa Fluor 488 goat anti-rabbit IgG, Alexa Fluor 488 rabbit anti-mouse IgG, Alexa Flour 488 rabbit anti-goat IgG, and Alexa Flour 488 goat anti-rabbit IgG were purchased from Invitrogen.

Plasmids

Human pIgR cDNA-containing pcDNA3.1 (+) was a generous gift from Dr Finn-Eirik Johansen (Rikshospitalet University Hospital, Oslo, Norway). The template sequences for pIgR short hairpin RNA (shRNA) were obtained using the Insert Design Tool for the pSilencer Vector of Ambion (Austin, TX). The template pIgR shRNA and non-silencing shRNA were chemically synthesized by GenePharma Co (Shanghai, China), annealed to form duplexes (90°C for 3 minutes followed by an incubation at 37°C for 1 hour), and subcloned into pSilencer2.1/Puro vector (Ambion) with T_4 DNA ligase at 14°C for 16 hours. Human pIgR mutants were generated using the Muta-direct Site-directed Mutagenesis kit (Beijing SBS Genetech Co, Ltd, Beijing, China). pBABE-puro-pIgR plasmids were constructed using recombinant polymerase chain reaction and subsequently were subcloned into the vectors. The polymerase chain reaction conditions were as follows: 94°C for 5 minutes; 30 cycles of 94°C for 1 minute, 60°C for 1 minute, and 72°C for 2.5 minutes; 72°C for 10 minutes. The polymerase chain reaction product was cloned into pBABE-puro vector at the EcoRI restriction site. All constructs were sequenced by Invitrogen.

Transfection and Infection

For stable transfections, MDCK cells were grown to 60% confluency in six-well plates and transfected with 4 μg of full-length pcDNA3.1 (+) vector or pcDNA3.1 (+)-pIgR, using 10 μL of Lipofectamine 2000 (Invitrogen) following the manufacturer's instructions. A monoclonal population of stably transfected cells was selected using 800 μg/mL geneticin (G418) (Invitrogen). MDCK-pIgR cells were grown to 60% confluency in six-well

plates and transfected with 4 μg full-length pSilencer2.1/Puro-con shRNA vector or the indicated pSilencer2.1/Puro-shRNA, using 10 μL of Lipofectamine 2000 following the manufacturer's instructions. A monoclonal population of stably transfected cells was selected using 2 μg/mL puromycin (Invitrogen). Transient transfection in MDCK and SMMC-7721 cells were performed as described above except that cells were directly harvested for analysis 48 hours after transfection.

For infection, phoenix cells (American Type Culture Collection) were grown in DMEM supplemented with 10% FBS to 60% confluency in 10-cm dishes and transfected with 24 μg of the retroviral constructs (described above) in antibiotic-free DMEM containing 10% FBS using 60 μL of Lipofectamine 2000 according to the manufacturer's instructions. Approximately 24 hours after transfection, the media was changed to fresh DMEM containing 10% FBS. After an additional 24-hour incubation at 37°C, the supernatant was collected, filtered using a 0.45-μm filter (Millipore, Cork, Ireland), and used to infect SMMC-7721 cells in the presence of 4 μg/mL polybrene (Millipore). Polyclonal populations of infected cells were then selected using 1 μg/mL puromycin.

RNA Interference

pIgR shRNAs were synthesized and cloned into a pSilencer2.1/Puro vector (Ambion). Target sequences for the shRNAs were as follows: pIgR shRNA1, 5′-GAACGUCGACCGAGUUUCA-3′; pIgR shRNA2, 5′-CGUCGACCGAGUUUCAAUC-3′; and pIgR shRNA3, 5′-GAAGAGUUUGUUGCCACCA-3′. Shanghai GenePharm (Shanghai, China) synthesized short interfering RNA (siRNAs) sequences specifically targeting human pIgR (5′-GAA GAGUUUGUUGCCACCATT-3′), human Smad2 (5′-GGU GUUCGAUAGCAUAUUATT-3′), human Smad3 (5′-GCCU GGUCAAGAAACUCAATT-3′), canine Smad2 (5′-ACAUAUA GGAAGAGGAGUATT-3′), canine Smad3 (5′-GAGGAGAAGU GGUGCGAGATT-3′), and non-targeting control siRNA (5′-UUCUCCGAACGUGUCACGUTT-3′). For siRNA delivery, double-stranded RNA oligonucleotides were transfected using Oligofectamine (Invitrogen). MDCK, HT29, or SMMC-7721 cells at 30%–50% confluency in six-well plates were transfected with 100 nM siRNAs, using 3 μL of Oligofectamine according to the manufacturer's instructions and harvested 48 hours after transfection for analysis.

Co-Immunoprecipitation and Immunoblot Analysis

For total protein extraction, the indicated cell lines were grown in six-well plates or 10-cm dishes; were lysed in buffer consisting of 25 mM HEPES (pH 7.5), 150 mM NaCl, 10 mM $MgCl_2 \cdot 6H_2O$, 0.1 mM EDTA, 1 mM sodium orthovanadate, 1% Nonidet P-40; and supplemented with a protease inhibitor cocktail (Roche, Indianapolis, IN) and then centrifuged at 12 000*g* at 4°C for 15 minutes. The supernatants containing the cellular proteins were then collected, and the protein concentration was measured using Bicinchoninic Acid Protein Assay Reagent (Pierce, Rockford, IL).

For co-immunoprecipitation, the protein lysates (1 mg) were incubated with the appropriate antibodies with rocking for 4 hours at 4°C, followed by the incubation of protein A/G plus Agarose (Santa Cruz Biotechnology) for 6 hours to overnight at 4°C with rocking. The beads were then washed with cold lysis buffer followed by centrifugation at 3000*g* at 4°C for 5 minutes. The bound proteins were then eluted using 0.2% sodium dodecyl sulfate.

Both total protein lysates and eluted proteins from the co-immunoprecipitation experiment were separated by sodium dodecyl sulfate polyacrylamide gel electrophoresis and transferred to Hybond C Extra nitrocellulose membranes (GE Healthcare, Chalfont, St Giles, UK). Membranes were incubated in blocking solution containing 5% dry milk or 1% bovine serum albumin for 1 hour at room temperature. The membranes were incubated at 4°C overnight with the appropriate primary antibodies (mouse anti-human E-cadherin antibody [dilution, 1:5000], rabbit anti-human Smad2 antibody [dilution, 1:1000], rabbit anti-human phospho-Smad2 [Ser465/467] antibody [dilution, 1:1000], rabbit anti-human Smad3 antibody [dilution, 1:1000], rabbit anti-human phospho-Smad3 [Ser423/425] antibody [dilution, 1:1000], mouse anti-human Snail antibody [dilution, 1:1000], mouse anti-human Slug antibody [dilution, 1:1000], mouse anti-human vimentin antibody [dilution, 1:2000], mouse anti-human fibronectin antibody [dilution, 1:1000], rabbit anti-human pIgR [H300] antibody [dilution, 1:1000], goat anti-human pIgR [N16] antibody [dilution, 1:1000], goat anti-human pIgR [C20] antibody [dilution, 1:1000], rabbit anti-Smad4 antibody [dilution, 1:1000], mouse anti-human pan-cytokeratin antibody [dilution, 1:100 000], rabbit anti-human β-actin antibody [dilution, 1:100 000], mouse anti-human TWIST1 antibody [dilution, 1:1000], mouse anti-human TWIST2 antibody [dilution, 1:1000], rabbit anti-human ZEB1 antibody [dilution, 1:1000], or mouse anti-human GAPDH antibody [dilution, 1:5000]). The membranes were washed for 15 minutes with Tris-buffered saline containing Tween 20 (TBST) (25 mM Tris, 150 mM NaCl, 2 mM KCl, pH 7.4, supplemented with 0.1% Tween 20) three times, before incubation at room temperature for 1 hour with horseradish peroxidase–conjugated anti-goat IgG (dilution, 1:2000), anti-rabbit IgG (dilution, 1:2000), or anti-mouse IgG (dilution, 1:2000) antibody. After washing the membranes with TBST three times for 15 minutes, bound antibodies were visualized using Western Blotting Luminal Reagent (Pierce) and subsequent exposure to KODAK X-OMAT BT Film (Kodak, Rochester, NY) for 30 seconds to 30 minutes. Immunoblotting for GAPDH or β-actin served as a protein loading control. All experiments were performed at least three independent times.

Experimental Lung Metastasis Model

Female severe combined immunodeficient (SCID) mice 6 weeks of age were supplied by the Shanghai Laboratory Animal Center, Chinese Academy of Sciences (Shanghai, China). Mice were housed five or six mice per cage in a specific pathogen-free room with a 12-hour light/dark schedule at 25°C ± 1°C and were fed an autoclaved chow diet and water ad libitum. All experiments were performed according to the institutional ethical guidelines on animal care and approved by the Institute Animal Care and Use Committee at Shanghai Institute of Materia Medica. The mice were randomly divided into indicated groups before the injection, and the double-blinded evaluation was performed when counting metastatic nodules.

The metastatic ability of pIgR-overexpressing MDCK and SMMC-7721 cells and respective control cells was determined following cell injection intravenously into the tail vein. MDCK cells (MDCK-mock, MDCK-pIgR, MDCK-pIgR-con.shRNA, or

MDCK-pIgR-shRNA3 cells) at 2×10^6 cells resuspended in 100 μL phosphate-buffered saline (PBS) were injected into the lateral tail veins of SCID mice (n = 5 mice per group). SMMC-7721-mock or SMMC-7721-pIgR cells (1×10^6 cells per mouse, resuspended in 100 μL PBS, n = 12 mice per group) were injected into the lateral tail veins of SCID mice. Sample size was calculated on the basis of 80% power. The number of mice per group was greater than the minimum numbers required as determined by a power test on the basis of preliminary studies—at least two mice per group were required for experiments with pIgR-overexpressing MDCK and control cells, whereas three mice per group were required for experiments with pIgR-overexpressing SMMC-7721 and control cells. In preliminary experiments, we observed a 60% change of death among mice injected with pIgR-overexpressing SMMC-7721 cells (data not shown); therefore, at least eight mice were needed to achieve 80% power. Survival was recorded daily. After 10 weeks, the mice were killed by CO_2, their lungs were removed, and the number of metastasis nodules on the lung surface was counted by the naked eye. Metastatic lungs were fixed with paraformaldehyde (4%) before dehydration and paraffin embedding. Paraffin sections were stained with hematoxylin and eosin according to standard protocols or were subjected to IHC staining using a horseradish peroxidase–labeled streptavidin–biotin ABC kit (ZSGB-BIO, Beijing, China) with hematoxylin as the counterstain.

Migration, Invasion, and Adhesion Assays

For wound-healing migration experiments, pIgR-overexpressing MDCK cell sets (MDCK-mock, MDCK-pIgR, MDCK-pIgR-con.shRNA, MDCK-pIgR-shRNA1, MDCK-pIgR-shRNA2, or MDCK-pIgR-shRNA3 cells) and pIgR-overexpressing SMMC-7721 cell sets (SMMC-7721-mock or SMMC-7721-pIgR cells) were grown to form a monolayer with 90% confluency. Cells were then scraped with a p200 tip (Axygen Scientific, Union City, CA), and medium was replaced with fresh RPMI-1640 medium supplemented with 2% FBS or DMEM medium supplemented with 2% FBS. Wound closure of the monolayered cells was monitored at the time of wounding (0 hour), and after 3, 6, and 9 hours with microphotographs at ×10 magnification using a Olympus IX51 research microscope with a DP-70 camera (both from Olympus, Tokyo, Japan). The experiment was performed three independent times in triplicate.

For the transwell assay, MDCK (1×10^5 cells) and SMMC-7721 cells (2×10^5 cells) were starved in serum- and growth factor-free medium for 12 hours and added to the top chambers of 24-well Transwell plates (8 μm; Corning Costar Corp, Corning, NY). The bottom chambers were filled with growth medium supplemented with 100 ng/mL secretory component (R&D Systems, Minneapolis, MN). Cultures were maintained for 48 hours, followed by removal of non-motile cells at the top of the filter with a cotton swab. Migrating cells were fixed in paraformaldehyde (4%) and stained with crystal violet (0.1%) for 15 minutes at room temperature. Dye that was taken up by cells bound to the membrane was released by addition of 100 μL 10% acetic acid, and the absorbance of the resulting solution was measured at 595 nm using a multiwell spectrophotometer (VERSAmax; Molecular Devices, Sunnyvale, CA). The assay was performed in triplicate and repeated twice.

For the matrigel invasion assay, pre-starved MDCK-mock, MDCK-pIgR, MDCK-pIgR-con.shRNA, MDCK-pIgR-shRNA1, MDCK-pIgR-shRNA2, or MDCK-pIgR-shRNA3 cells (5×10^4 cells per well) were cultured in the top chambers containing matrigel-coated membrane inserts. The bottom chambers were filled with RPMI-1640 medium supplemented with 10% FBS. After incubation for a further 48 hours, cells were fixed in paraformaldehyde (4%) and stained with crystal violet (0.1%) for 15 minutes at room temperature, and images at ×10 magnification were taken using the Olympus IX51 research microscope with a DP-70 camera. The assay was performed three independent times in triplicate.

For the adhesion assay, MDCK-mock, MDCK-pIgR, MDCK-pIgR-con.shRNA, MDCK-pIgR-shRNA1, MDCK-pIgR-shRNA2, or MDCK-pIgR-shRNA3 cells (3×10^4 cells per well) were cultured in fibronectin-coated 96-well plates in triplicate for 1 hour at 37°C. After gentle washing with PBS, non-adherent cells were discarded, and adherent cells were fixed with 5% glutaraldehyde and stained with 0.1% crystal violet. Dye that was taken up by cells bound to the membrane was dissolved in 100 μL 10% acetic acid, and the absorbance was measured at 595 nm using a multiwell spectrophotometer (VERSAmax; Molecular Devices). The experiment was performed three independent times.

Urokinase-Type Plasminogen Activator (uPA)-Plasmingen Assay

MDCK (1.5×10^3 cells per well) and SMMC-7721 (6×10^3 cells per well) cells stably overexpressing an empty vector or pIgR cDNA were seeded in 96-well plates and grown overnight at 37°C. Then cells were cultured in fresh medium for 24 hours. Alternatively, HT29 cells were seeded at 6000 cells per well in 96-well plates and grown overnight at 37°C. Fresh medium containing tumor necrosis factor α (TNF-α) (5, 10, 20 ng/mL) (Peprotech Inc, Rocky Hill, NJ) was added to the appropriate wells and incubated for 24 hours at 37°C. The plates were processed for determination of plasminogen activity by first rinsing twice with phenol red–free DMEM and then adding 200 μL of reaction buffer containing 50% (vol/vol) 0.05 units/mL plasminogen (Roche) in phenol red–free DMEM, 40% (vol/vol) 50 mM Tris–HCl pH 8.2, 10% (vol/vol) 3 mM Chromozyme PL (Roche), and 0.2% tween 20 in 100 mM glycine solution to each well. The plates were incubated for 6 hours at 37°C, 5% CO_2, and the absorbance of each well was read using an automated spectrophotometric plate reader (VERSAmax; Molecular Devices) at 405 nm. The results were repeated in three independent experiments.

Immunocytochemistry

pIgR-overexpressing MDCK cell sets (MDCK-mock, MDCK-pIgR, MDCK-pIgR-con.shRNA, MDCK-pIgR-shRNA1, MDCK-pIgR-shRNA2, or MDCK-pIgR-shRNA3 cells) or pIgR-overexpressing SMMC-7721 cell sets (SMMC-7721-mock or SMMC-7721-pIgR cells) were plated onto 24-well glass chamber slides (20 000 or 10 000 cells per well) and incubated at 37°C in a humidified incubator with 5% CO_2 for 36 hours. The cells were fixed with 4% formaldehyde at room temperature for 1 hour and permeabilized with 0.1% Triton X-100 in PBS at room temperature for 5 minutes. Subsequently, cells were washed three times for 5 minutes each using PBS containing 1% bovine serum albumin. Cells were incubated with primary antibodies (mouse anti-human E-cadherin antibody [dilution, 1:100], mouse anti-human pan-cytokeratin

antibody [dilution, 1:100], mouse anti-human vimentin antibody [dilution, 1:100], or mouse anti-human fibronectin antibody [dilution, 1:100]). For dual immunostaining, the primary antibodies were goat anti-human pIgR (C20) antibody (dilution, 1:100), rabbit anti-human Smad2 antibody (dilution, 1:1000), rabbit anti-human Smad3 antibody (dilution, 1:1000), and mouse anti-human EEA1 antibody (dilution, 1:100). The cells were washed three times for 5 minutes each using PBS containing 1% bovine serum albumin and then incubated with Alexa Fluor 546 goat anti-mouse IgG (dilution, 1:1000) or Alexa Fluor 488 rabbit anti-mouse IgG (dilution, 1:1000) for single immunofluorescence staining and with Alexa Fluor 546 goat anti-mouse IgG (dilution, 1:1000) and Alexa Flour 488 rabbit anti-goat IgG (1:1000 dilution), or Alexa Fluor 546 goat anti-mouse IgG (dilution, 1:1000) and Alexa Flour 488 goat anti-rabbit IgG (1:1000 dilution) for dual immunofluorescence staining at room temperature for 1 hour. Cells were observed using a Zeiss LS510 confocal microscope (Carl Zeiss, Jena, Germany) at ×400 magnification for single immunofluorescence experiments and an Olympus FV 1000 confocal microscope at ×600 magnification for dual immunofluorescence experiments. All experiments were repeated three independent times.

Statistical Analysis

All data (except tissue microarray and animal survival analyses) were analyzed using Student *t* test. Statistical analysis of tissue microarrays was performed using the statistical package SPSS (version 16.0; SPSS Inc, Chicago, IL). DFS and Overall survival were assessed using the Kaplan–Meier method and compared with the log-rank test. Fisher exact test was applied to determine clinicopathologic correlations. Univariable and multivariable risk ratios were computed with 95% confidence intervals (CIs). Univariable risk ratios with 95% confidence intervals were calculated using Cox proportional hazards regression models with forward stepwise selection (forward likelihood ratio). Models were adjusted by serum gamma glutamyl transferase (>54 or ≤54 U/L), α-fetoprotein (>20 or ≤20 U/L), tumor encapsulation (none or complete), tumor size (>5 or ≤5 cm), the number of tumors (multiple or single), vascular invasion (yes or no), TNM stage (stage I or stages II–III), Barcelona Clinic Liver Cancer group stage (stages 0–A or stages B–D), pIgR (low or high expression, on the basis of a score ranging from 0 to 4 [low] and 6 to 8 [high]). Multivariable risk ratios with 95% confidence intervals were calculated using Cox multivariable analysis and Cox proportional hazards regression models. Covariables were adopted for their prognostic significance by univariate analysis ($P < .05$) with forward stepwise selection (forward likelihood ratio). Mouse survival analysis was analyzed using the Kaplan–Meier method and compared using the log-rank test. All statistical tests were two-sided, and *P* values less than .05 were considered statistically significant.

Results

pIgR Expression in HCC Patients With Early Tumor Recurrence

We analyzed 254 tumor specimens from HCC patients for whom follow-up data was available after they underwent curative hepatectomy. Of these HCC patients, 211 (83.1%) tested positive for hepatitis B surface antigen (HBsAg), an indicator of HBV infection (Supplementary Table 1, available online). The tumor specimens were grouped according to high- and low-levels of pIgR expression, and 98 specimens (38.6%) belonged to the high-expression group. Patients with high pIgR expression had a statistically significantly higher risk of early tumor recurrence as indicated by the decreased DFS compared with HCC patients with low levels of pIgR expression (log-rank $P = .02$, Figure 1, A; hazard ratio = 1.64, 95% CI = 1.08 to 2.48, likelihood ratio test $P = .02$, Supplementary Table 2, available online, respectively). When stratified by sex, we found that high-level expression of pIgR was statistically significantly associated with a higher risk of early recurrence, shown as decreased DFS in male HCC patients, as compared with female HCC patients (log-rank $P = .03$ vs .57, respectively) (data not shown). Multivariable analyses adjusting for the clinicopathologic variables were adopted for their prognostic significance ($P < .05$) by univariate analyses, which further confirmed that high expression of pIgR was an independent prognostic predictor of early tumor recurrence in HCC patients (hazard ratio = 1.61, 95% CI = 1.07 to 2.45, $P = .02$) (Table 1).

HBV-related carcinogenesis is a multistep process, encompassing the combination of different not mutually exclusive effects such as the induction of chronic liver inflammation and regeneration (37). HBsAg positivity indicates a clear HBV infection and harbors a higher risk to develop HCC, whereas the positivity of hepatitis B e antigen (HBeAg) usually indicates active HBV replication (38). When stratified by HBV viral status, we found that high-level expression of pIgR was statistically significantly associated with a higher risk of early recurrence, shown as decreased DFS in HBsAg-positive HCC patients, as compared with HBsAg-negative patients (log-rank $P = .02$ vs .62, respectively) (Figure 1, B). A similar but non-statistically significant trend was also observed in HBeAg-positive patients (HBeAg-positive vs HBeAg-negative HCC patients, log-rank $P = .05$ vs .14) (Supplementary Figure 1, A, available online). These findings suggest that HBsAg-associated chronically active inflammation may lead to increased pIgR protein expression that subsequently promotes tumor early recurrence.

Because loss of E-cadherin expression, a hallmark of EMT, is noted in many malignancies and is associated with metastatic potential (39–41), we examined E-cadherin levels using IHC staining and analyzed the relationship between E-cadherin and pIgR expression. High-level pIgR expression was statistically significantly associated ($P = .02$) with loss of E-cadherin (69.8%) (pIgR high expression level patients vs pIgR low expression level patients, E-cadherin weak positive rate = 69.8% vs 45.7%, difference = 24.1%, 95% CI of the difference = 4.2% to 44.0%) (Figure 1, C) in HCC specimens showing early tumor recurrence. Figure 1, D shows the corresponding representative IHC-stained tissue sections. This inverse association between pIgR and E-cadherin expression was also confirmed by immunoblotting (Supplementary Figure 1, B, available online). In addition, high-level expression of pIgR was also associated with reduced expression of another epithelial marker, pan-cytokeratin, and with an elevated level of the mesenchymal marker, vimentin (Supplementary Figure 1, B, available online). Such a specific expression pattern suggests a role for pIgR in EMT induction in HCC patients.

High expression of pIgR remained statistically significantly associated with DFS and its reflecting early tumor recurrence in

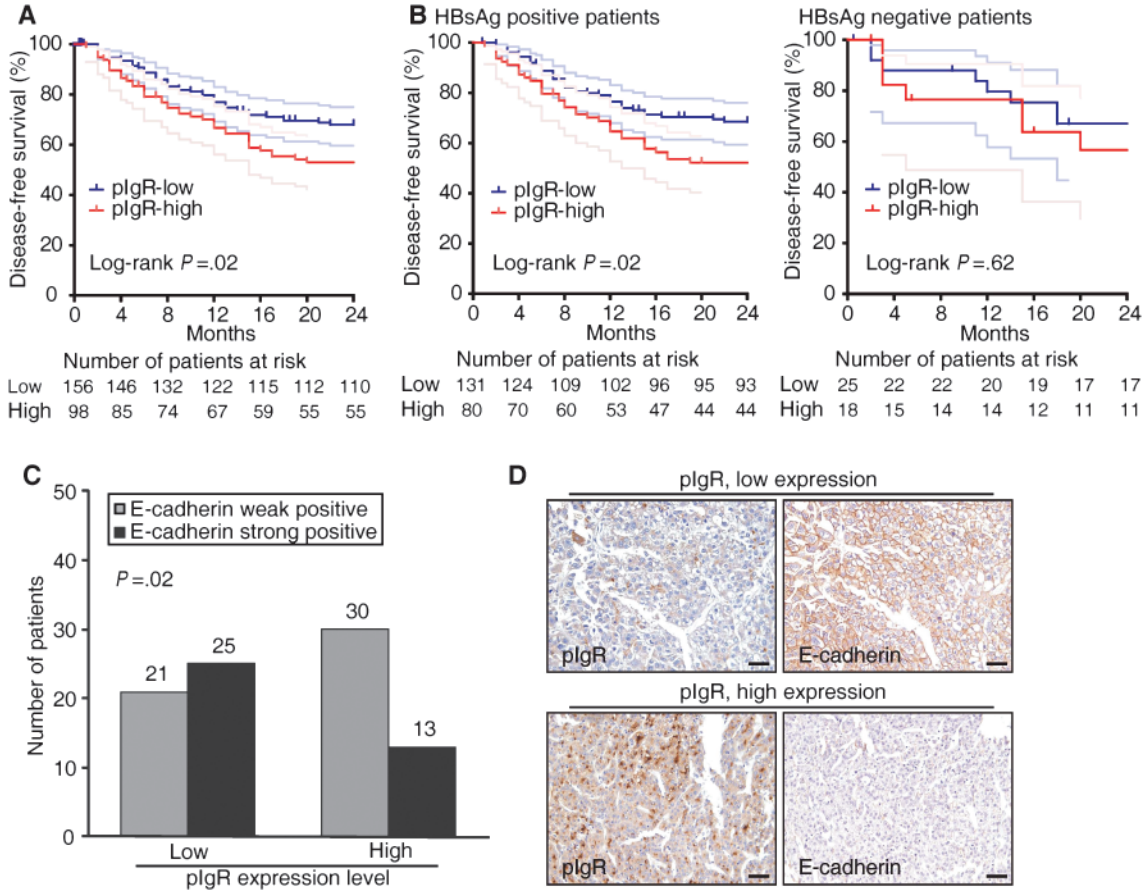

Figure 1. Association between polymeric immunoglobulin receptor (pIgR) expression and poor prognosis and relationship between pIgR and E-cadherin expression level in hepatocellular carcinoma (HCC) patients after resection. **A**) Comparison of disease-free survival (DFS) (indicating early tumor recurrence, recurrence ≤2 years after resection) in HCC patients with high and low expression levels of pIgR. Kaplan–Meier survival analysis was performed, and *P* was calculated using a two-sided log-rank test. DFS rates with 95% confidence intervals (**light color lines**) in patients with pIgR high or low expression are shown. The absolute number of patients at risk is listed below the curve. **B**) Kaplan–Meier survival analysis of hepatitis B surface antigen (HBsAg)–positive and HBsAg-negative HCC patients by pIgR expression (high or low) was performed, and *P* values were calculated using a two-sided log-rank test. DFS rates with 95% confidence intervals (**light color lines**) in patients with pIgR high or low expression are shown. The absolute number of patients at risk is listed below the curve. **C**) E-cadherin expression patterns (weak or strong positive staining) were analyzed in HCC patients with high (n = 43) vs low (n = 46) pIgR who had early recurrence using the two-sided Fisher exact test. **D**) Representative immunostained images of pIgR and E-cadherin protein expression in HCC tissues (**scale bars** = 50 μm).

this scenario in patients with early stages of HCC when further stratified by the level of vascular invasion (*P* = .03), the number of tumors (*P* = .004), tumor size (*P* = .03), and TNM stage (*P* = .005) (Figure 2, A–D, left panel). In contrast, pIgR expression was not statistically significantly associated with DFS in patients with late-stage HCC when stratified using these same variables (Figure 2, A–D, right panel). Because early recurrence is most likely the consequence of occult metastasis from the initial tumor (31,33), our data suggest that high-level pIgR expression is closely associated with a higher risk of metastasis, particularly in patients at early stages of HCC. These results further suggest that pIgR may serve as an important tumor metastatic factor predicting metastatic potential in the clinic, particularly in the early stages of HCC.

Relationship Between pIgR Expression and EMT Induction In Vitro

To confirm the role of pIgR in EMT, we used a model epithelial cell line, MDCK, to generate six stable cell lines, one overexpressing pIgR (MDCK-pIgR) and the other five with pIgR shRNA knockdown (MDCK-pIgR-shRNA1, shRNA2, shRNA3) and controls (MDCK-pIgR-con.shRNA and MDCK-mock). Parental MDCK cells exhibit a cobblestone morphology in monolayer cultures with tight cell–cell contacts, characteristic of epithelial cells. However, MDCK cells with elevated expression of pIgR showed loss of cell–cell contact and displayed a spindle-like fibroblastic morphology, one of the principal characteristics of EMT (Figure 3, A). Such morphological changes were accompanied by almost complete loss of the epithelial markers E-cadherin and pan-cytokeratin (Figure 3, B, and Supplementary Figure 2, A, available online) and by increased expression of the mesenchymal markers vimentin and fibronectin (Figure 3, B, and Supplementary Figure 2, A, available online). The mesenchymal phenotype, including cellular morphology and the expression pattern of mesenchymal markers, displayed by the pIgR high-expressing MDCK cells was almost completely reversed by shRNA knockdown of pIgR (Figure 3, A–B, and Supplementary Figure 2, A, available online), indicating that pIgR is required for

Table 1. Multivariable analyses of factors associated with DFS in 254 hepatocellular carcinoma patients*

Variables†	DFS‡ HR (95% CI)	*P*§
Tumor number (multiple vs single)	1.76 (1.07 to 2.92)	.03
Vascular invasion (yes vs no)	2.28 (1.49 to 3.48)	<.001
pIgR (high vs low)	1.61 (1.07 to 2.45)	.02

* CI = confidence interval; DFS = disease-free survival; HR = hazard ratio; pIgR = polymeric immunoglobulin receptor.

† Cox multivariable analysis and Cox proportional hazards regression models were used. Variables were adopted for their prognostic significance by univariable analysis ($P < .05$) with forward stepwise selection (forward likelihood ratio).

‡ For patients who had a confirmed tumor recurrence, DFS was calculated as the time that early recurrence (≤2 years) was first suspected. DFS was used as surrogate endpoint for indicating early recurrence.

§ *P* values were calculated using a two-sided likelihood ratio test.

induction of EMT in MDCK cells. Furthermore, high expression of pIgR was also sufficient to induce EMT in two hepatic carcinoma cell lines: SMMC-7721 (Figure 3, A–B) and BEL-7404 (data not shown), as well as a normal liver cell line LO2 (data not shown), when these cell lines were induced to transiently or stably overexpress pIgR.

We next examined whether cell motility was affected by pIgR-induced EMT. Overexpression of pIgR resulted in a clear and potent migratory phenotype as assessed by a wound-healing assay in both SMMC-7721 (pIgR vs mock, mean migration distance at 6 hours = 56.9 vs 15.5 μm; mean difference = 41.4 μm, 95% CI of the difference = 11.0 to 71.8 μm, $P = .004$; similar results were observed at 3 and 9 hours) (Figure 3, C) and MDCK cells (pIgR vs mock, mean migration distance at 6 hours = 81.5 vs 30.9 μm, mean difference = 50.6 μm, 95% CI of the difference = 35.7 to 65.5 μm, $P < .001$; similar results were observed at 3 and 9 hours) (Figure 3, D). Matrigel invasion studies also revealed that MDCK-pIgR cells were statistically significantly more invasive compared with MDCK-mock cells (Supplementary Figure 2, B, available online). Furthermore, high-level expression of pIgR was associated with a statistically significant decrease in cell adhesion (Supplementary Figure 2, C, available online). In agreement with these findings, overexpression of pIgR in MDCK and SMMC-7721 cells dramatically activated uPA activity (Figure 3, E), a hallmark of cancer cell invasion and metastasis (42,43). Conversely, pIgR knockdown in pIgR-overexpressing MDCK cells reversed the migratory phenotypes, as shown in the wound-healing assay (pIgR shRNA1 vs pIgR con.shRNA, mean migration distance at 6 hours = 70.8 vs 80.1 μm, mean difference = −9.3 μm, 95% CI of the difference = −14.5 to −4.1 μm, $P = .14$; pIgR shRNA2 vs pIgR con.shRNA, mean migration distance at 6 hours = 48.0 vs 80.1 μm, mean difference = −32.1 μm, 95% CI of the difference = −64.0 to −0.2 μm, $P = .004$; pIgR shRNA3 vs pIgR con.shRNA, mean migration distance at 6 hours = 38.3 vs 80.1 μm, mean difference = −41.8 μm, 95% CI of the difference = −46.6 to −37.0 μm, $P = .001$; similar results were observed at 3 and 9 hours) (Figure 3, D). Similar results were observed in matrigel invasion assay and adhesion assay (Supplementary Figure 2, B–C, available online).

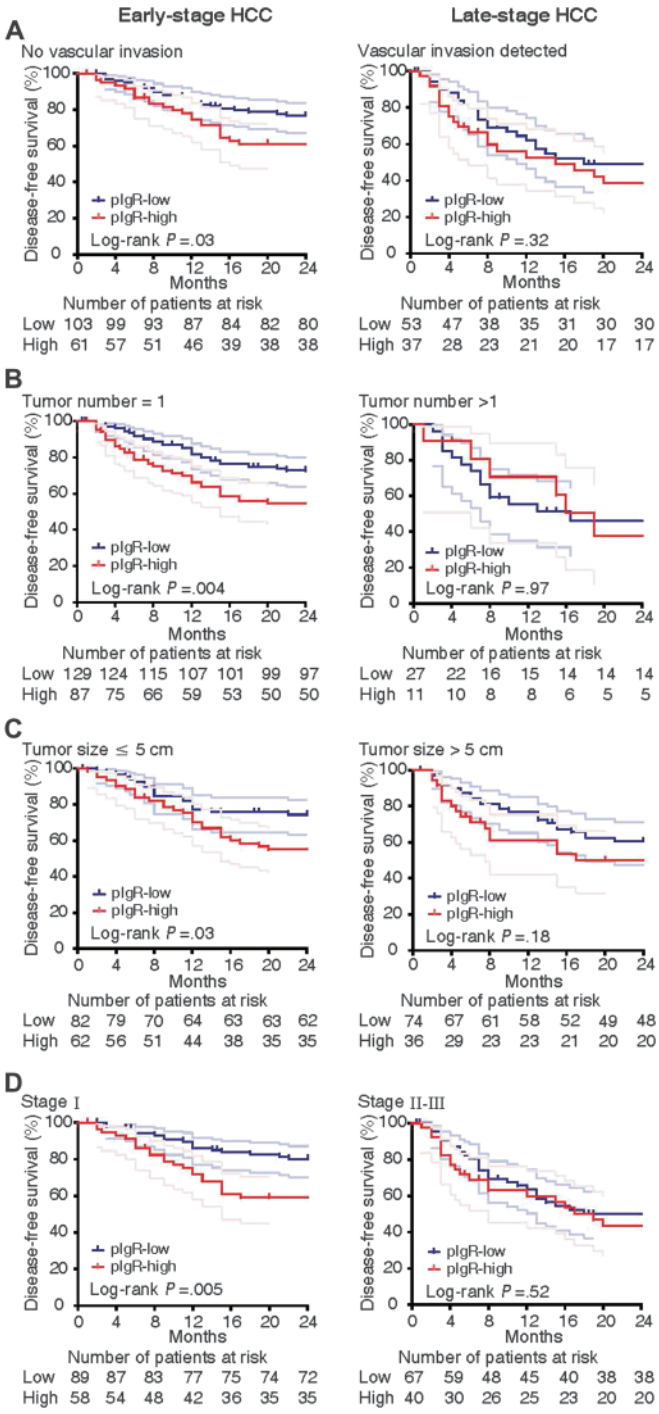

Figure 2. The prognostic significance of polymeric immunoglobulin receptor (pIgR) expression stratified by hepatocellular carcinoma stage. Kaplan–Meier survival analysis of early- and late-stage patients with high or low pIgR expression stratified by **A**) vascular invasion (present or not present), **B**) tumor number (1 or >1 tumor), **C**) tumor size (≤5 or >5 cm), and **D**) TNM stage (stage I or II–III). Disease-free survival rates with 95% confidence intervals (**light color lines**) in patients with pIgR high or low expression are shown. The absolute number of patients at risk is listed below each curve. *P* values were calculated using a two-sided log-rank test.

Effect of Proinflammatory Cytokines on pIgR Expression and Its Association with EMT

Expression of pIgR is commonly increased by proinflammatory cytokines, including TNF-α, interferon γ (IFN-γ), and interleukin

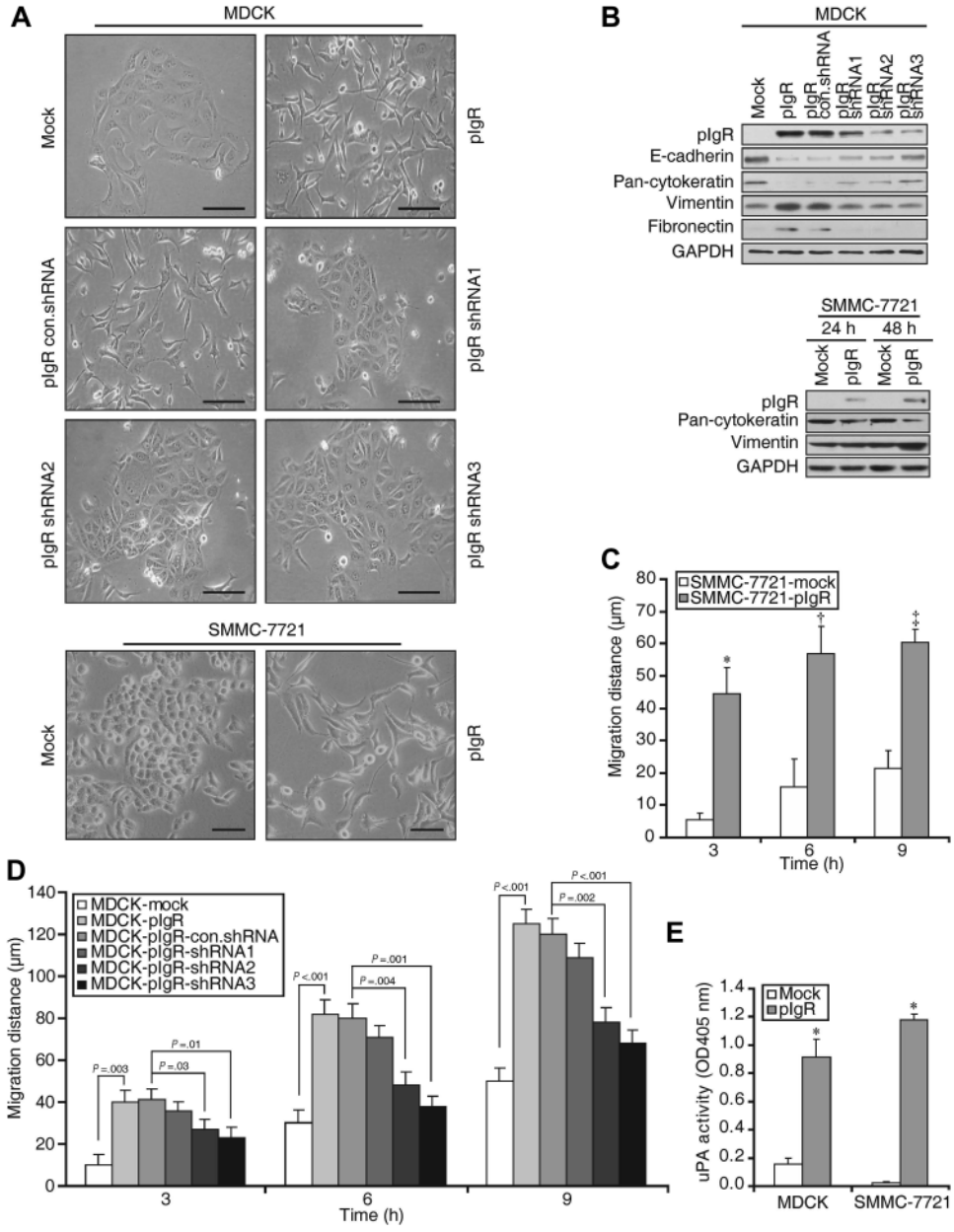

Figure 3. Effect of polymeric immunoglobulin receptor (pIgR) expression on induction of epithelial–mesenchymal transition. **A**) Morphology of Madin–Darby canine kidney (MDCK) (**top panel**) and SMMC-7721 (**bottom panel**) cells stably expressing pIgR cDNA alone or pIgR short hairpin RNA (shRNA) plus pIgR cDNA (**scale bar** = 50 μm). **B**) Immunoblot analysis of MDCK cells stably expressing pIgR (**top panel**) and SMMC-7721 cells transiently expressing pIgR (**bottom panel**). Experiments were repeated three times with similar results. glyceraldehyde-3-phosphate dehydrogenase (GAPDH) was used as a loading control. **C**) The migration distance of SMMC-7721 cells stably expressing pIgR cDNA alone or pIgR cDNA plus pIgR shRNA was analyzed using a wound-healing assay. Data from three independent experiments performed in triplicate are presented as the mean with the SD (**error bars**). * $P = .001$, † $P = .004$, ‡ $P < .001$, vs the mock-transfected (control) cells. **D**) The migration distance of MDCK cells stably expressing pIgR cDNA alone or pIgR cDNA plus pIgR shRNA was analyzed using a wound-healing assay. Data from three independent experiments performed in triplicate are presented as the mean with the SD (**error bars**). All *P* values were calculated using the two-sided Student *t* test. **E**) Urokinase-type plasminogen activator (uPA) activation in MDCK and SMMC-7721 cells stably expressing pIgR cDNA was investigated. Data from three independent experiments performed in triplicate are presented as the mean with the SD (**error bars**). * $P < .001$, vs mock. All *P* values were calculated using the two-sided Student *t* test. OD = optical density.

4 (IL-4), in response to viral or bacterial infections (16,17,19,44). Having established that high expression of pIgR was associated with early recurrence of chronically HBV-infected HCC patients, and increased pIgR expression induced EMT, we next asked whether elevated pIgR expression by the stimulation of proinflammatory cytokines could induce EMT induction in vitro. To this end, we chose a model cell line, human colonic adenocarcinoma HT29, which can respond well to the stimulation of cytokines in terms of increasing pIgR expression (16,17). We exposed the HT29 cell line to various concentrations of proinflammatory cytokines and, as expected, exposure to high concentrations of TNF-α, IL-4, or IFN-γ increased expression of pIgR and vimentin and

decreased expression of E-cadherin in a dose-dependent and time-dependent manner (Figure 4, A–C). Moreover, knockdown of pIgR in TNF-α-treated HT29 cells triggered a decrease in vimentin and an increase in E-cadherin (Figure 4, D). Together, these data indicate that proinflammatory cytokines induce expression of pIgR, which in turn activates EMT, a critical step for inflammation-initiated tumor progression. In TNF-α-stimulated HT29 cells, a statistically significant increase in pIgR expression was also accompanied by increased uPA activity (Figure 4, E), further supporting the role of pIgR in EMT induction.

Effect of pIgR Overexpression on Metastatic Lesions In Vivo

To determine the in vivo consequences of pIgR overexpression, we injected MDCK-mock, MDCK-pIgR, MDCK-pIgR-con.shRNA, or MDCK-pIgR-shRNA3 cells into the lateral tail veins of SCID mice (n = 5) and evaluated the survival of cells in circulation and their metastatic growth in the lung. After 10 weeks, the MDCK-pIgR-injected mice displayed a statistically significantly higher number of lung metastases than mice injected with MDCK-mock cells (pIgR mean = 29.4 metastatic nodules per lung vs control mean = 0.0 metastatic nodules per lung, difference = 29.4 metastatic nodules per lung, 95% confidence interval = 13.0 to 45.8, $P = .001$), indicative of extravasation to and tumor growth in the lung (Figure 5, A and B). When lungs underwent hematoxylin and eosin staining, lung metastases were observed in all five mice intravenously injected MDCK-pIgR cells, whereas no obvious lung metastases were observed in the mice intravenously injected MDCK-mock cells (Figure 5, C shows representative hematoxylin- and eosin-stained lung sections). In contrast, MDCK-pIgR-shRNA3

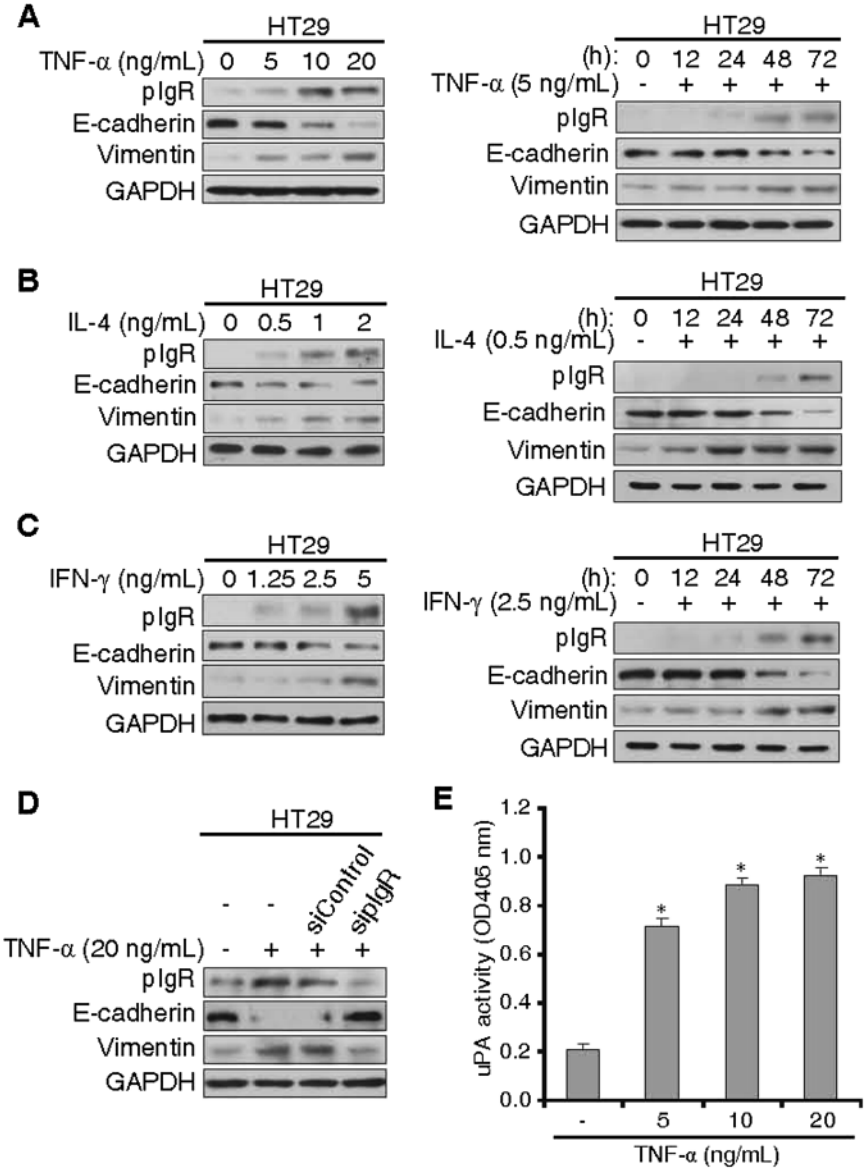

Figure 4. The effect of polymeric immunoglobulin receptor (pIgR) up-regulation by proinflammatory cytokines on induction of epithelial–mesenchymal transition in HT29 cells. HT29 cells treated with the indicated concentrations of **A**) TNF-α, **B**) IL-4, or **C**) IFN-γ in serum-free medium for 48 hours (left panels) or after treatment in serum-free medium for 0, 12, 24, 48, and 72 hours (right panels) underwent immunoblot for pIgR, E-cadherin, and vimentin expression. Glyceraldehyde-3-phosphate dehydrogenase (GAPDH) was used as a loading control. The experiment was repeated three times with similar results. **D**) pIgR siRNA3-transfected HT-29 cells were treated with TNF-α in serum-free medium for 48 hours and analyzed by immunoblotting for pIgR, E-cadherin, vimentin, and GAPDH (loading control). Data are representative of three independent experiments. **E**) urokinase-type plasminogen activator (uPA) activation in HT29 cells treated with TNF-α for 48 hours was determined. Data from three independent experiments performed in triplicate are presented as the mean with SD (**error bars**). *$P < .001$ vs untreated HT29 cells, as calculated using the two-sided Student t test. IFN-γ = interferon γ; IL-4 = interleukin 4; siRNA = short interfering RNA; TNF-α = tumor necrosis factor α.

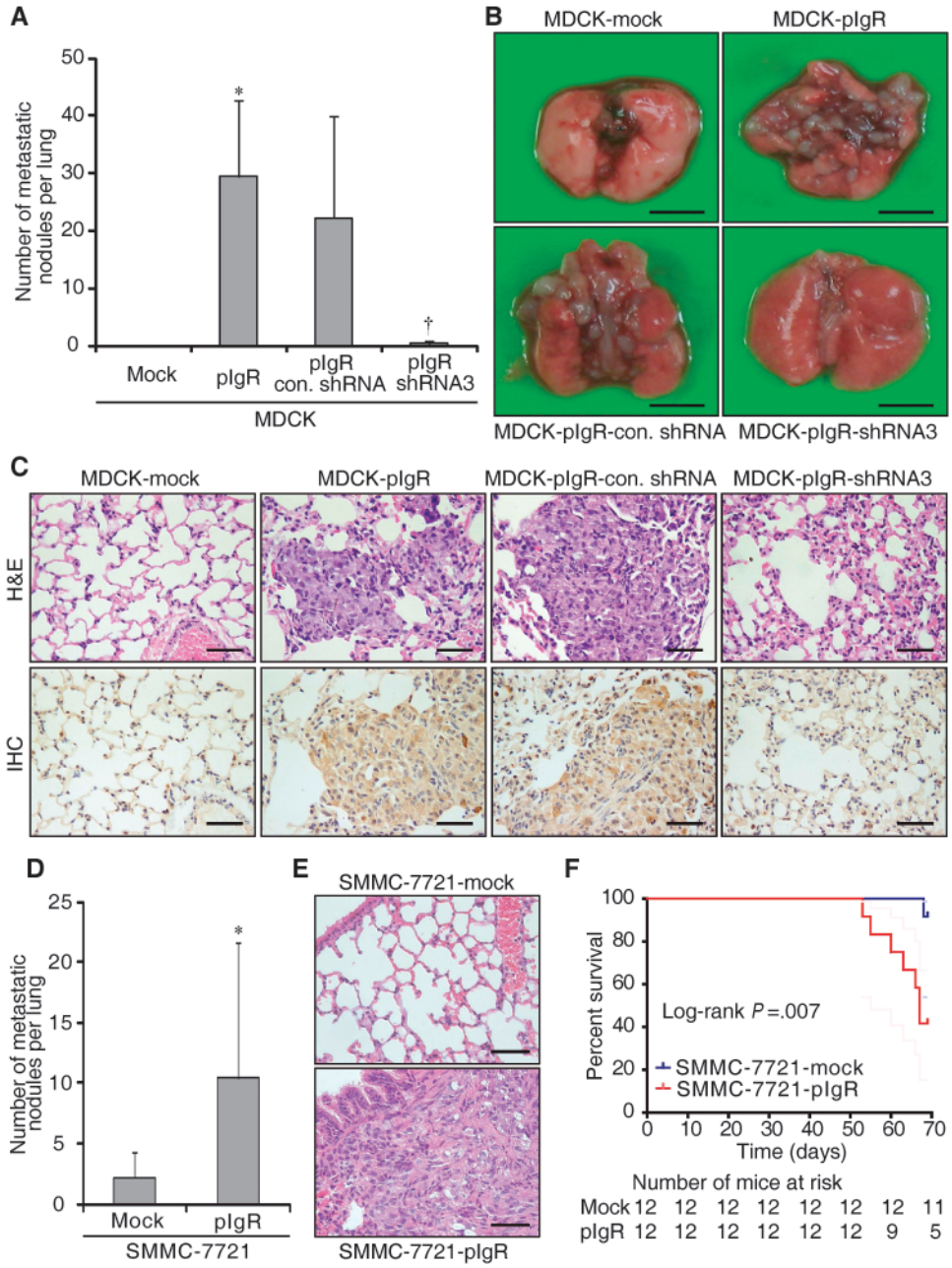

Figure 5. Effect of polymeric immunoglobulin receptor (pIgR) overexpression on metastasis in vivo. The metastatic abilities of Madin–Darby canine kidney (MDCK) cells stably expressing an empty vector (Mock), pIgR cDNA, pIgR cDNA plus control (non-targeting) short hairpin RNA (shRNA), or pIgR cDNA plus pIgR shRNA3 were examined in severe combined immunodeficient (SCID) mice via tail vein injection. **A**) The number of metastatic nodules on the surface of the lungs of mice injected with the MDCK cells (n = 5 mice per group) was determined. Data are presented as the mean and SD (**error bars**). **P* = .001 vs the mock group, and † *P* = .03 vs the pIgR con.shRNA group. All *P* values were calculated using the two-sided Student *t* test. This experiment was repeated three times with similar results. **B**) Representative images of lungs on day 70 after mice were injected with MDCK stable transfectants (**scale bar** = 5 mm). **C**) Representative images of hematoxylin and eosin (H&E) and immunohistochemical staining of pIgR in lung tissues of mice injected with MDCK stable transfectants (**scale bar** = 50 μm, at ×40 magnification) are shown. **D–F**) The metastatic abilities of SMMC-7721 cells stably expressing empty vector (mock) or pIgR cDNA were examined in SCID mice via tail vein injection. **D**) Number of metastatic nodules on the surface of the lungs of mice injected with SMMC-7721 transfectants (n = 11 mice in the mock group and n = 5 mice in the pIgR group) are presented as the mean and SD (**error bars**). **P* = .03 vs the mock group, calculated by the two-sided Student *t* test. **E**) Representative images of H&E stained of lung tissues from mice injected with SMMC-7721 transfectants (**scale bar** = 50 μm). **F**) The comparison of survival curves of mice injected with either SMMC-7721-pIgR or SMMC-7721-mock vectors. Survival rates with 95% confidence intervals (**light color lines**) in mice injected with either SMMC-7721-pIgR or SMMC-7721-mock vectors are shown. *P* was calculated by the two-sided log-rank test. The absolute number of mice at risk is listed below the curve. The last column number indicates the number of mice at risk on day 69. IHC = immunohistochemistry.

cells did not metastasize or had statistically significantly fewer metastatic nodules per lung (pIgR shRNA3 vs pIgR con.shRNA, mean number of metastatic nodules per lung = 0.4 vs 22.2 nodules, mean difference = −21.8 nodules, 95% CI of the difference = −43.3 to −0.3 nodules, *P* = .03) (Figure 5, A–C). Similar results were obtained in mice injected with liver cancer cells that have pIgR

overexpression (SMMC-7721-pIgR cells: pIgR mean = 10.4 metastatic nodules per lung vs control mean = 2.2 metastatic nodules per lung, difference = 8.2 metastatic nodules per lung, 95% confidence interval = 1.0 to 15.5, $P = .03$) (Figure 5, D–E). These mice had a statistically significantly shorter survival rate (survival rate analysis of mice intravenously injected pIgR-overexpressing SMMC-7721 cells, pIgR vs mock, survival rate = 41.7% vs 91.7%, difference = −50%, 95% CI of the difference = −82.0% to −18.0%, $P = .007$) compared with mice that were injected with SMMC-7721 cells with barely detectable expression of pIgR (Figure 5, F). Our data thus indicate that pIgR is necessary for the development of the aggressive and highly metastatic phenotype.

Relationship Between pIgR Overexpression and Activation of Smad Signaling

To determine the molecular basis of how pIgR induces EMT, we focused on the Smad signaling pathway that is known to play a major role in EMT induction. Increased expression of pIgR in MDCK and SMMC-7721 cells caused a dramatic activation of Smad2/3 compared with the mock control–treated cells (Figure 6, A). Similar results were obtained for TNF-α-, IL-4-, and IFN-γ-treated HT29 cells (Supplementary Figure 3, A–C, available online). To further confirm the ability of pIgR to induce Smad activation, we used shRNAs or siRNA to knock down pIgR expression. Knockdown of pIgR resulted in a substantial decrease in phosphorylated Smad 2/3 in pIgR-overexpressing MDCK cells (Figure 6, A) and in TNF-α-treated HT29 cells (Supplementary Figure 3, D, available online), suggesting that pIgR was required for Smad activation. Because transforming growth factor β (TGF-β), a known Smad canonical stimuli, synergizes with proinflammatory cytokines in EMT induction (14,45–48), we introduced TGF-β to MDCK-pIgR, SMMC-7721-pIgR, and TNF-α-stimulated HT29 cells. We found that TGF-β caused a dramatic increase in Smad2/3 phosphorylation and vimentin expression and a decreased in E-cadherin expression, when compared with the TGF-β-untreated pIgR high-expressing cells at both 24 and 48 hours (Figure 6, B and Supplementary Figure 3, E, available online). These data indicated that TGF-β and pIgR converged in activating Smad2/3 as part of EMT induction.

We next determined whether pIgR-induced EMT was mediated by Smad activation. Transfection of MDCK-pIgR or SMMC-7721-pIgR cells with either Smad2/3 or Smad2 siRNAs almost completely reversed the pIgR-driven EMT as measured by an increase in E-cadherin and cytokeratin and a decrease in vimentin levels (Figure 6, C). Smad3 siRNAs also inhibited pIgR-directed EMT but to a lesser extent compared with Smad2 knockdown. These data indicate that activation of Smads, particularly Smad2, is essential for pIgR-induced EMT.

To determine whether pIgR promotes Smad activation in vivo, we examined Smad2/3 phosphorylation in HCC samples. Increased levels of phospho-Smad2/3 were observed in pIgR-overexpressing HCC samples that exhibited EMT characteristics (Supplementary Figure 1, B, available online), indicating that high levels of pIgR expression lead to increased Smad activation and EMT induction.

Mechanism of Smad Activation by pIgR

To determine how pIgR activates Smad, we tested whether pIgR plays a direct role in recruiting the Smad signaling complex. Using immunofluorescence assay in pIgR-expressing MDCK and SMMC-7721 cells, we found that overexpression of pIgR increased Smad2/3 nuclear translocation (Supplementary Figure 4, A and B, available online). More importantly, we found that pIgR, Smad2, and Smad3 were colocalized extensively with EEA1, an early endosome marker (Supplementary Figure 4, A and B, available online). Specifically, pIgR and Smad2/3 were present in the same endocytic compartment, the EEA1-positive early endosome. This finding is consistent with a previous report that both pIgR and Smad2/3 are localized to EEA1-positive early endosomes (18,49–52). Furthermore, endogenous Smad2/3 was immunoprecipitated with an anti-pIgR antibody from cell lysates from MDCK-pIgR cells and pIgR transiently expressing SMMC-7721 cells, and vice versa (Figure 6, D). These reciprocal co-immunoprecipitation data suggest that pIgR activates Smad signaling by recruiting the Smad2/3 complex. To identify which component is the direct target of pIgR, we repeated the co-immunoprecipitation with lysates from MDCK-pIgR cells and pIgR transiently overexpressing SMMC-7721 cells after treatment with siRNA for Smad2 or Smad3. Knockdown of Smad2, but not Smad3, led to disruption of pIgR-Smad interactions, suggesting that pIgR plays a direct role in recruiting Smad2 (Figure 6, E). We also found that endogenous pIgR interacted with endogenous Smad2/3 in HT29 cells after exposure to IL-4 (Supplementary Figure 3, F, available online). Together, our data suggest that pIgR is a novel partner of the Smad complex and that it activates Smad signaling by recruiting Smad2.

We also found that expression of pIgR increased the protein levels of Snail, Slug, and ZEB1, but not Twist1/2, which are all key E-cadherin repressors required for EMT (40,47). Knockdown of pIgR in MDCK pIgR-expressing cells resulted in a dramatic reversion in the expression pattern of these E-cadherin repressors (Supplementary Figure 5, A−B, available online). These data suggest that pIgR-mediated Smad activation converges on the EMT signaling pathways regulated by the Snail, Slug, and ZEB1 transcription factors.

The Role of Serines 682 and 734 in the Cytoplasmic Tail of pIgR in EMT Induction

Our results so far have established that pIgR has a signaling role in EMT induction in addition to its classic function as a transporter of dIgA and pIgM. To further map which residues in the cytoplasmic domain of pIgR are essential for signaling in EMT induction, we performed a series of point mutations in tyrosine residues 677 and 743 and serine residues 673, 682, 734, and 735, because phosphorylation of these residues is likely to play a signaling role in pIgR-mediated EMT induction. Tyrosine 677 and 743 and serine 673 and 735 are known to play critical roles in transcytosis, a key step in transportation of dIgA and pIgM by pIgR during the immune response (18,53–55). However, mutations of Y677F, Y743F, S673A, and S735A had little effect on the ability of pIgR to induce EMT in MDCK and SMMC-7721 cells (Figure 7, A and Supplementary Figure 6, A, available online). In addition, the cleaved extracellular domain of pIgR, which is responsible for binding to dIgA and pIgM, failed to induce EMT (Supplementary Figure 6, B–C, available online). Together, these data indicate that the major residues required for pIgR-mediated immunoglobulin

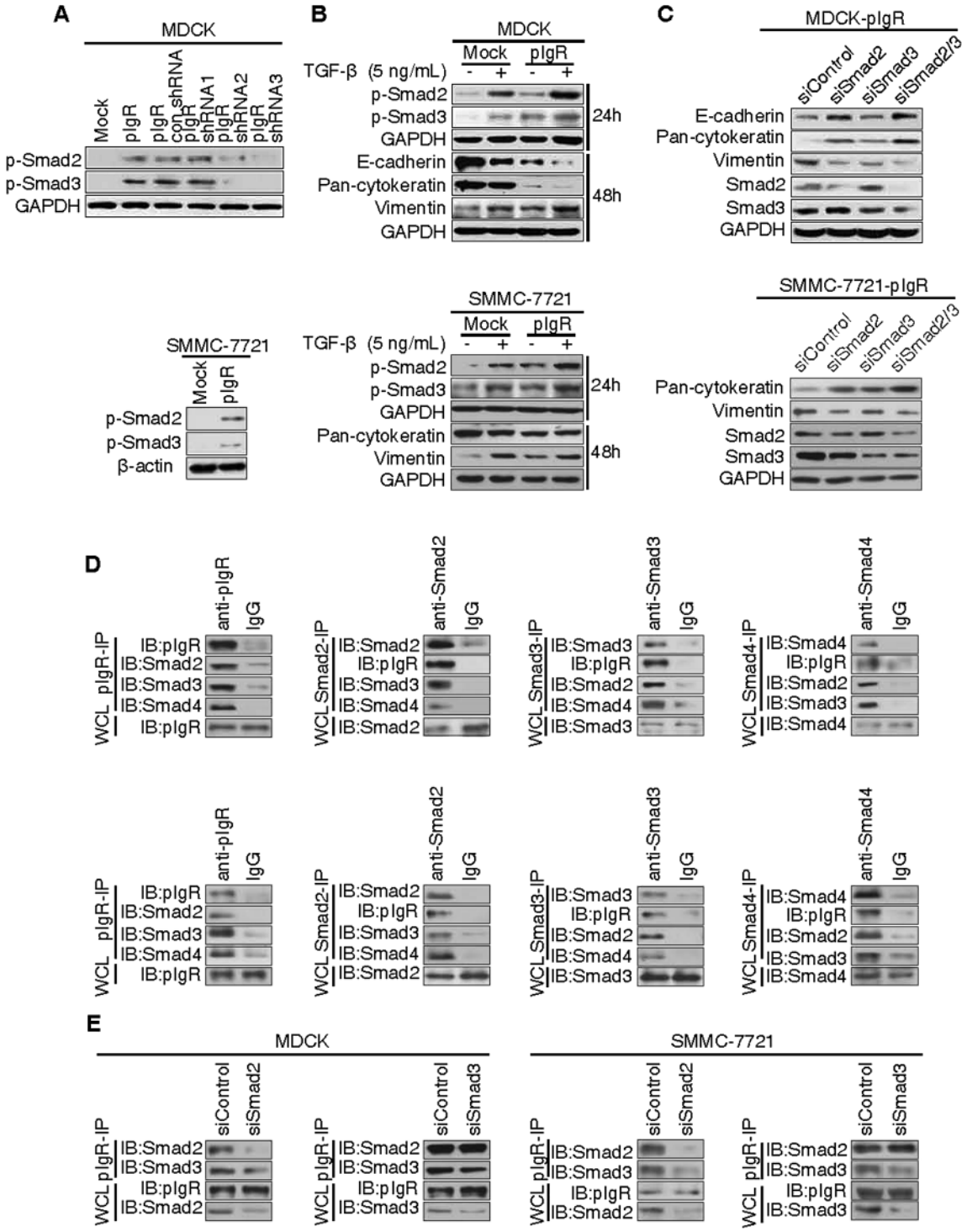

Figure 6. Activation of Smad signaling by polymeric immunoglobulin receptor (pIgR). **A**) Protein lysates from Madin–Darby canine kidney (MDCK) cells stably expressing pIgR cDNA or pIgR cDNA plus pIgR short hairpin RNA (shRNA) (**top panel**) and SMMC-7721 cells transiently expressing pIgR cDNA (**bottom panel**) were immunoblotted for phospho-Smad2 and phospho-Smad3 (p-Smad2 and p-Smad3, respectively). Glyceraldehyde-3-phosphate dehydrogenase (GAPDH) and β-actin served as a loading control. **B**) MDCK stable transfectants (**top panel**) and SMMC-7721 transient transfectants (**bottom panel**) underwent immunoblotting for p-Smad2 and pSmad3 24 hours after treatment with TGF-β (5 ng/mL) or were immunoblotted for E-cadherin, pan-cytokeratin, and vimentin 48 hours after transforming growth factor-β (TGF-β) treatment. GAPDH served as a loading control. **C**) Immunoblots of epithelial and mesenchymal markers and activated Smad2 and Smad 3 in MDCK stable transfectants (**top panel**) and SMMC-7721 transient transfectants (**bottom panel**) after a separate transfection with Smad2 and Smad3 siRNAs. **D**) Co-immunoprecipitation of Smads and pIgR from whole-cell lysates (WCL) prepared from MDCK cells (**top panel**) and SMMC-7721 cells (**bottom panel**) as described in (**A**). Co-immunoprecipitation with IgG served as a negative control. **E**) Anti-pIgR immunoprecipitates from Smad2 or Smad3 depleted–MDCK cells stably expressing pIgR (**left panel**) and SMMC-7721 cells transiently expressing pIgR (**right panel**) were analyzed by immunoblotting for Smads and pIgR. All images are representative of data from three independent experiments. IP = immunoprecipitation; siRNA = short interfering RNA.

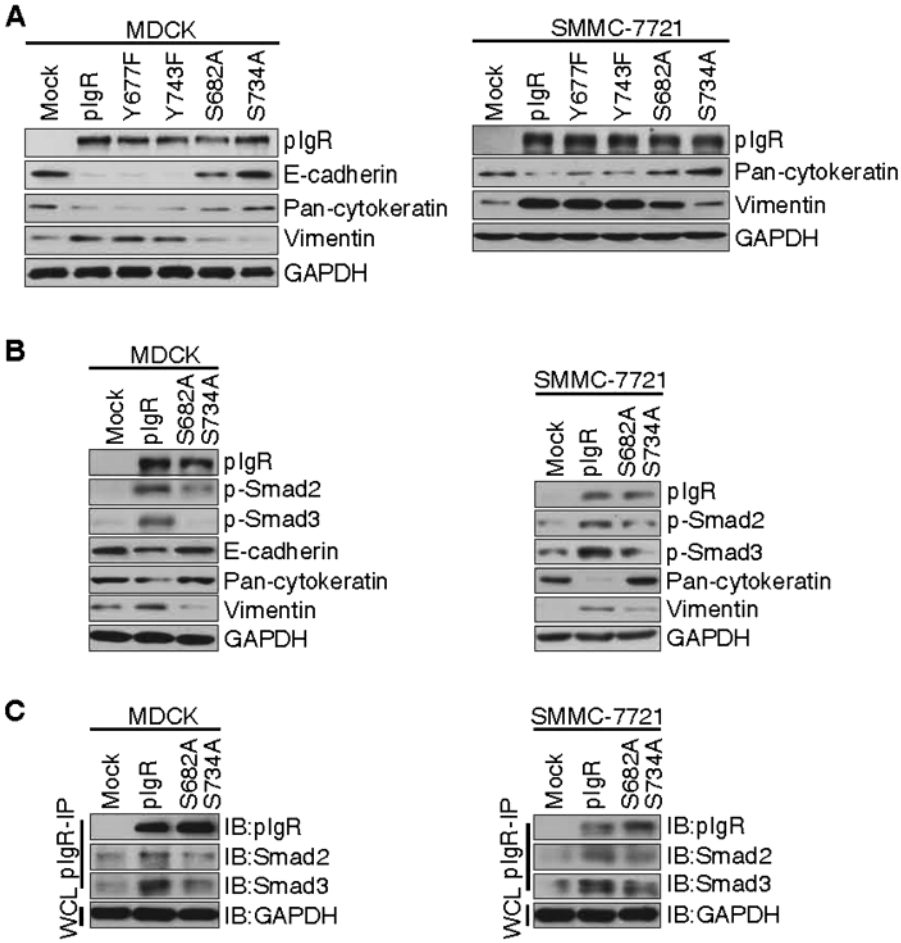

Figure 7. Identification of the serine residue in the cytoplasmic tail of polymeric immunoglobulin receptor (pIgR) that is necessary for the induction of epithelial–mesenchymal transition. **A**) Madin–Darby canine kidney (MDCK) (**left panel**) and SMMC-7721 (**right panel**) cells transiently transfected with empty vector (mock), wild-type pIgR, or the indicated pIgR mutants were analyzed using immunoblotting for epithelial and mesenchymal markers. **B**) MDCK (**left panel**) and SMMC-7721 (**right panel**) cells transiently transfected with an empty vector (mock) or indicated pIgR mutants were analyzed by immunoblot for activated Smad2 and Smad3, and E-cadherin, pan-cytokeratin, and vimentin. **C**) Anti-pIgR immunoprecipitates from MDCK (**left panel**) and SMMC-7721 (**right panel**) cells transiently transfected with empty vector (mock), wild-type pIgR, or the indicated pIgR mutant were analyzed by immunoblot for Smad2, Smad3, and pIgR. Glyceraldehyde-3-phosphate dehydrogenase (GAPDH) served as a loading control for all experiments. Similar results were seen in three independent experiments. IP = immunoprecipitation; WCL = whole-cell lysates.

transportation differ from those required for pIgR-mediated EMT induction.

In contrast, mutations in serine residues 682 and 734 (S682A/S734A and S734A) nearly abolished the ability of pIgR to induce EMT (Figure 7, A–B), suggesting that these residues are critical for pIgR-induced EMT. Given the essential role of Smad activation in pIgR-driven EMT, we tested whether S682 and S734 participated in pIgR-directed Smad activation. Whereas wild-type pIgR induced Smad2/3 phosphorylation, the S682A/S734A double mutant failed to induce Smad2/3 phosphorylation in MDCK or SMMC-7721 cells (Figure 7, B). Furthermore, the S682A/S734A double mutation substantially reduced interactions between pIgR and Smad2/3 (Figure 7, C). These findings suggest that serine residues at positions 734 and 682 are not only required for pIgR binding to Smads but also for Smad activation that leads to EMT induction.

Discussion

In this study, we demonstrated that pIgR is a signaling mediator of HBV-related hepatitis and HCC metastasis. High expression of pIgR was inversely associated with DFS and was associated with poor prognosis in HCC patients. Data showed that the pIgR expression level may indicate the metastatic potential of early-stage HCC. Mechanistically, pIgR induced the EMT process in vitro and in vivo through activation of Smad signaling. These results establish a missing link between hepatitis-related chronic inflammation, EMT, and HCC metastasis.

It is well known that inflammatory immune responses to HBV viral antigens induce hepatocyte damage, followed by the regeneration of hepatocytes and the development of fibrosis and cirrhosis, which are the important features in pathogenesis of HCC (37,56). In fact, HBsAg positivity indicates a clear HBV infection; and HBeAg positivity usually reflects active replication with ongoing inflammation and progression of HCCs. In this study, we showed that high-level pIgR in HBsAg-positive patients was associated with a higher risk of early recurrence in HCC patients, indicating that the chronic HBV viral infection in hepatitis-related HCC causes the changes of microenvironment such as the release of proinflammatory cytokines that increase pIgR expression to promote HCC metastasis. Indeed, we also observed a statistically significant association between TNF-α and pIgR expression in HCC patients who had early recurrence, indicated by shorter DFS (data not shown). Notably, in the same specimens from early-recurrence HCC patients, increased pIgR levels are accompanied by a loss of E-cadherin, the hallmark of EMT, indicative of the clinical significance of pIgR in promoting tumor recurrence and metastasis via EMT induction. The proinflammatory cytokines TNF-α, IL-4, and IFN-γ were observed to increase pIgR and promote a clear EMT induction. Our data presented here show that pIgR is involved in EMT induction and may be a mechanistic link between hepatitis-related chronic inflammation and HCC

metastasis, indicating that chronic inflammation to HCC is a decisive factor in EMT induction in HCC metastasis (14,57).

The mainstream view of inflammation and cancer is currently focused on inflammatory cytokines such as TNF-α and their associated signaling pathways. Identification of pIgR as a signaling mediator of inflammation-induced EMT provides a missing link between HBV-related chronic inflammation and HCC metastasis. To the best of our knowledge, pIgR is the first example of a well-known immunoglobulin receptor involved in HBV-related hepatitis-mediated EMT and HCC metastasis. The discovery of this new role could provide a basis for the study of novel mechanisms underlying inflammation-mediated HCC progression.

The important mechanistic finding from our study is that pIgR-induced EMT is mediated by the activation of Smad complex. pIgR activates Smad signaling by recruiting Smad2/3 complex, which is consistent with the fact that both pIgR and Smad2/3 are colocalized in EEA1-postive early endosomes, in which pIgR participates in transcytosis during the immune response (18,52) and Smad2/3 are activated for signal transduction (49–51). The ability of pIgR to activate Smad signaling suggests that pIgR functions as a novel partner of the Smad2/3 signaling complex and establishes the first link between a known immunoglobulin receptor and the Smad signaling pathway. Integrating all the results, we propose a signaling pathway from inflammation to EMT induction. In this pathway, inflammation induced by infections or tumor microenvironments leads to chronic production of cytokines such as TNF-α, which results in overexpression of pIgR and activation of Smad signaling that in turn leads to EMT induction and tumor metastasis.

Generally, the transport of dIgA and pIgM by pIgR is mediated by the ligand binding to the extracellular domain and by transcytosis that requires the cytoplasmic tail of pIgR (18,19). Our mutagenesis studies revealed that different structural elements are required for the transport function and for the EMT induction, respectively. Mutations in tyrosine and serine residues (Y677F and Y743F; S673A and S735A) that are important for transcytosis do not affect EMT function of pIgR, but mutations in two serine residues (S682A and S734A) unrelated to transcytosis nearly abolish the ability of pIgR to induce EMT, suggesting that transcytosis and EMT induction of pIgR are mediated through two distinct signaling pathways. The critical function of S682 and S734 in pIgR-mediated EMT induction also suggests that phosphorylation of these residues may play an important role, and the exact signaling pathways leading to their phosphorylation warrant future investigation. The new role of pIgR in EMT revealed in this study suggests that pIgR has at least two functions: one as the transporter of dIgA and pIgM and the other as a signaling molecule for inflammation-induced EMT.

Establishing the role of pIgR in EMT also helps to resolve the long-standing conflict on the clinical relevance of pIgR in tumor progression (23,24,58–62). This is a reminiscent of the debate about the significance of EMT in tumor progression and its relevance in human cancers, which was not established until recently because EMT is transient and reversible (10,63,64). We observed a statistically significant association between high but not low expression of pIgR and the metastatic risk for early (but not late) stages of HCC, suggesting that pIgR-driven EMT is indeed a transient event at the early stages of HCC. This observation is consistent with previous hypotheses that metastasis is not necessarily a late event in tumor progression (10,65). The discrepancy regarding pIgR expression and clinical relevance in various tumors may be resolved if the stages of the tumors and the subtle characteristics of EMT, which are easily overlooked in clinical samples, are taken into account.

Our study has a few limitations. Although we have noted a clear trend that high expression of pIgR is associated with the early recurrence in HBeAg-positive HCC patients, it was not statistically significant, most likely because of the limited number of patients enrolled in the study. An expanded patient cohort will probably validate this observation. Moreover, our novel findings that increased pIgR expression promotes EMT have expanded the understanding of the role of pIgR in cancer metastasis, but the detailed regulatory network is presumably far more expansive than what our study has shown. It, therefore, will be important to carry out further investigations to identify additional signaling modulators and delineating pivotal regulatory mechanisms involving pIgR and metastasis.

In summary, we demonstrate that pIgR is a novel signaling mediator of HBV-related chronic inflammation–induced tumor metastasis via EMT induction besides its normal function as a transporter of IgA and IgM. Given a major obstacle for the poor prognosis of HCC is recurrence and metastasis after surgery or ablation therapy (4–7), identification of pIgR as a predictor of metastatic potential in early-stage HCC patients could facilitate patient stratification and therapeutic decisions at early stage, therefore affecting the clinical outcome. Our study not only reveals a missing link between HBV-related chronic inflammation and HCCs metastasis but also provides a potential predictive biomarker for prognosis of HCC and a potential therapeutic target.

References

1. Yang JD, Roberts LR. Hepatocellular carcinoma: a global view. *Nat Rev Gastroenterol Hepatol.* 2010;7(8):448–458.
2. Finn RS. Development of molecularly targeted therapies in hepatocellular carcinoma: where do we go now? *Clin Cancer Res.* 2010;16(2):390–397.
3. Jemal A, Siegel R, Ward E, et al. Cancer statistics, 2008. *CA Cancer J Clin.* 2008;58(2):71–96.
4. El-Serag HB, Marrero JA, Rudolph L, et al. Diagnosis and treatment of hepatocellular carcinoma. *Gastroenterology.* 2008;134(6):1752–1763.
5. Fan ST. Selection of HCC patients for liver transplantation: the Milan criteria, Hangzhou criteria and beyond. *Hepatobiliary Pancreat Dis Int.* 2008;7(3):233–234.
6. De Giorgio M, Fagiuoli S. Management of hepatocellular carcinoma. *Dig Dis.* 2007;25(3):279–281.
7. Kudo M, Okanoue T. Management of hepatocellular carcinoma in Japan: consensus-based clinical practice manual proposed by the Japan Society of Hepatology. *Oncology.* 2007;72(suppl 1):2–15.
8. Cheung ST, Cheung PF, Cheng CK, et al. Granulin-epithelin precursor and ATP-dependent binding cassette (ABC)B5 regulate liver cancer cell chemoresistance. *Gastroenterology.* 2011;140(1):344–355.
9. Friedman SL. Mechanisms of hepatic fibrogenesis. *Gastroenterology.* 2008;134(6):1655–1669.
10. Thiery JP, Acloque H, Huang RY, et al. Epithelial-mesenchymal transitions in development and disease. *Cell.* 2009;139(5):871–890.
11. Mani SA, Guo W, Liao MJ, et al. The epithelial-mesenchymal transition generates cells with properties of stem cells. *Cell.* 2008;133(4):704–715.
12. Ansieau S, Bastid J, Doreau A, et al. Induction of EMT by twist proteins as a collateral effect of tumor-promoting inactivation of premature senescence. *Cancer Cell.* 2008;14(1):79–89.

13. Kudo-Saito C, Shirako H, Takeuchi T, et al. Cancer metastasis is accelerated through immunosuppression during Snail-induced EMT of cancer cells. *Cancer Cell.* 2009;15(3):195–206.
14. Lopez-Novoa JM, Nieto MA. Inflammation and EMT: an alliance towards organ fibrosis and cancer progression. *EMBO Mol Med.* 2009;1(6–7):303–314.
15. van Zijl F, Zulehner G, Petz M, et al. Epithelial-mesenchymal transition in hepatocellular carcinoma. *Future Oncol.* 2009;5(8):1169–1179.
16. Denning GM. IL-4 and IFN-gamma synergistically increase total polymeric IgA receptor levels in human intestinal epithelial cells. Role of protein tyrosine kinases. *J Immunol.* 1996;156(12):4807–4814.
17. Kvale D, Lovhaug D, Sollid LM, et al. Tumor necrosis factor-alpha up-regulates expression of secretory component, the epithelial receptor for polymeric Ig. *J Immunol.* 1988;140(9):3086–3089.
18. Rojas R, Apodaca G. Immunoglobulin transport across polarized epithelial cells. *Nat Rev Mol Cell Biol.* 2002;3(12):944–955.
19. Kaetzel CS. The polymeric immunoglobulin receptor: bridging innate and adaptive immune responses at mucosal surfaces. *Immunol Rev.* 2005; 206(1):83–99.
20. Poger ME, Hirsch BR, Lamm ME. Synthesis of secretory component by colonic neoplasms. *Am J Pathol.* 1976;82(2):327–338.
21. Harris JP, South MA. Secretory component: a glandular epithelial cell marker. *Am J Pathol.* 1981;105(1):47–53.
22. Harris JP, Caleb MH, South MA. Secretory component in human mammary carcinoma. *Cancer Res.* 1975;35(7):1861–1864.
23. Rossel M, Seilles E, Voigt JJ, et al. Polymeric Ig receptor expression in hepatocellular carcinoma. *Eur J Cancer.* 1992;28A(6–7):1120–1124.
24. Kvale D, Norstein J, Meling GI, et al. Circulating secretory component in relation to early diagnosis and treatment of liver metastasis from colorectal carcinomas. *J Clin Pathol.* 1992;45(7):568–571.
25. Yang XR, Xu Y, Shi GM, et al. Cytokeratin 10 and cytokeratin 19: predictive markers for poor prognosis in hepatocellular carcinoma patients after curative resection. *Clin Cancer Res.* 2008;14(12):3850–3859.
26. Gao Q, Qiu SJ, Fan J, et al. Intratumoral balance of regulatory and cytotoxic T cells is associated with prognosis of hepatocellular carcinoma after resection. *J Clin Oncol.* 2007;25(18):2586–2593.
27. Edmondson HA, Steiner PE. Primary carcinoma of the liver: a study of 100 cases among 48,900 necropsies. *Cancer.* 1954;7(3):462–503.
28. Child CG, Turcotte JG. Surgery and portal hypertension. In: Child CG, ed. *The Liver and Portal Hypertension.* Philadelphia, PA: Saunders; 1964: 50–64.
29. Greene FL, Page DL, Fleming ID, et al. *AJCC Cancer Staging Manual.* 6th ed. New York, NY: Springer; 2002.
30. Hoshida Y, Villanueva A, Kobayashi M, et al. Gene expression in fixed tissues and outcome in hepatocellular carcinoma. *N Engl J Med.* 2008; 359(19):1995–2004.
31. Poon RT. Differentiating early and late recurrences after resection of HCC in cirrhotic patients: implications on surveillance, prevention, and treatment strategies. *Ann Surg Oncol.* 2009;16(4):792–794.
32. Portolani N, Coniglio A, Ghidoni S, et al. Early and late recurrence after liver resection for hepatocellular carcinoma: prognostic and therapeutic implications. *Ann Surg.* 2006;243(2):229–235.
33. Sherman M. Recurrence of hepatocellular carcinoma. *N Engl J Med.* 2008; 359(19):2045–2047.
34. Llovet JM, Di Bisceglie AM, Bruix J, et al. Design and endpoints of clinical trials in hepatocellular carcinoma. *J Natl Cancer Inst.* 2008;100(10):698–711.
35. Sotiriou C, Wirapati P, Loi S, et al. Gene expression profiling in breast cancer: understanding the molecular basis of histologic grade to improve prognosis. *J Natl Cancer Inst.* 2006;98(4):262–272.
36. Davidson B, Trope CG, Wang TL, et al. Expression of the chromatin remodeling factor Rsf-1 is upregulated in ovarian carcinoma effusions and predicts poor survival. *Gynecol Oncol.* 2006;103(3):814–819.
37. Zhou H, Wang H, Zhou D, et al. Hepatitis B virus-associated intrahepatic cholangiocarcinoma and hepatocellular carcinoma may hold common disease process for carcinogenesis. *Eur J Cancer.* 2010;46(6):1056–1061.
38. Yang HI, Lu SN, Liaw YF, et al. Hepatitis B e antigen and the risk of hepatocellular carcinoma. *N Engl J Med.* 2002;347(3):168–174.
39. Wu Y, Deng J, Rychahou PG, et al. Stabilization of snail by NF-kappaB is required for inflammation-induced cell migration and invasion. *Cancer Cell.* 2009;15(5):416–428.
40. Yang J, Weinberg RA. Epithelial-mesenchymal transition: at the crossroads of development and tumor metastasis. *Dev Cell.* 2008;14(6): 818–829.
41. Zeisberg M, Neilson EG. Biomarkers for epithelial-mesenchymal transitions. *J Clin Invest.* 2009;119(6):1429–1437.
42. Mekkawy AH, Morris DL, Pourgholami MH. Urokinase plasminogen activator system as a potential target for cancer therapy. *Future Oncol.* 2009;5(9):1487–1499.
43. Dass K, Ahmad A, Azmi AS, et al. Evolving role of uPA/uPAR system in human cancers. *Cancer Treat Rev.* 2008;34(2):122–136.
44. Johansen FE, Brandtzaeg P. Transcriptional regulation of the mucosal IgA system. *Trends Immunol.* 2004;25(3):150–157.
45. Bates RC, Mercurio AM. Tumor necrosis factor-alpha stimulates the epithelial-to-mesenchymal transition of human colonic organoids. *Mol Biol Cell.* 2003;14(5):1790–1800.
46. Massague J. TGFbeta in Cancer. *Cell.* 2008;134(2):215–230.
47. Polyak K, Weinberg RA. Transitions between epithelial and mesenchymal states: acquisition of malignant and stem cell traits. *Nat Rev Cancer.* 2009;9(4):265–273.
48. Takahashi E. Tumor necrosis factor-α regulates transforming growth factor-β-dependent epithelial-mesenchymal transition by promoting hyaluronan-CD44-moesin interaction. *J Biol Chem.* 2010;285(6):4060–4073.
49. Di Guglielmo GM, Le Roy C, Goodfellow AF, et al. Distinct endocytic pathways regulate TGF-beta receptor signalling and turnover. *Nat Cell Biol.* 2003;5(5):410–421.
50. Hayes S, Chawla A, Corvera S. TGF beta receptor internalization into EEA1-enriched early endosomes: role in signaling to Smad2. *J Cell Biol.* 2002;158(7):1239–1249.
51. Hu Y, Chuang JZ, Xu K, et al. SARA, a FYVE domain protein, affects Rab5-mediated endocytosis. *J Cell Sci.* 2002;115(pt 24):4755–4763.
52. Leung SM, Ruiz WG, Apodaca G. Sorting of membrane and fluid at the apical pole of polarized Madin-Darby canine kidney cells. *Mol Biol Cell.* 2000;11(6):2131–2150.
53. Okamoto CT, Shia SP, Bird C, et al. The cytoplasmic domain of the polymeric immunoglobulin receptor contains two internalization signals that are distinct from its basolateral sorting signal. *J Biol Chem.* 1992;267(14):9925–9932.
54. Casanova JE, Breitfeld PP, Ross SA, et al. Phosphorylation of the polymeric immunoglobulin receptor required for its efficient transcytosis. *Science.* 1990;248(4956):742–745.
55. Okamoto CT, Song W, Bomsel M, et al. Rapid internalization of the polymeric immunoglobulin receptor requires phosphorylated serine 726. *J Biol Chem.* 1994;269(22):15676–15682.
56. El-Serag HB, Rudolph KL. Hepatocellular carcinoma: epidemiology and molecular carcinogenesis. *Gastroenterology.* 2007;132(7):2557–2576.
57. Grivennikov SI, Greten FR, Karin M. Immunity, inflammation, and cancer. *Cell.* 2010;140(6):883–899.
58. Traicoff JL, De Marchis L, Ginsburg BL, et al. Characterization of the human polymeric immunoglobulin receptor (PIGR) 3'UTR and differential expression of PIGR mRNA during colon tumorigenesis. *J Biomed Sci.* 2003;10(6 pt 2):792–804.
59. Koretz K, Schlag P, Quentmeier A, et al. Evaluation of the secretory component as a prognostic variable in colorectal carcinoma. *Int J Cancer.* 1994;57(3):365–370.
60. Kawai T, Torikata C, Suzuki M. Immunohistochemical study of pulmonary adenocarcinoma. *Am J Clin Pathol.* 1988;89(4):455–462.
61. Isaacson P. Immunoperoxidase study of the secretory immunoglobulin system in colonic neoplasia. *J Clin Pathol.* 1982;35(1):14–25.
62. Kondi-Paphitis A, Addis BJ. Secretory component in pulmonary adenocarcinoma and mesothelioma. *Histopathology.* 1986;10(12):1279–1287.
63. Kalluri R. EMT: when epithelial cells decide to become mesenchymal-like cells. *J Clin Invest.* 2009;119(6):1417–1419.
64. Lu J, Guo H, Treekitkarnmongkol W, et al. 14-3-3zeta Cooperates with ErbB2 to promote ductal carcinoma in situ progression to invasive breast

cancer by inducing epithelial-mesenchymal transition. *Cancer Cell.* 2009; 16(3):195–207.
65. Husemann Y, Geigl JB, Schubert F, et al. Systemic spread is an early step in breast cancer. *Cancer Cell.* 2008;13(1):58–68.

Funding

This research was supported by grants from the Natural Science Foundation of China for Distinguished Young Scholars (30725046 to MG), the Natural Science Foundation of China for Innovation Research Group (81021062 to JD), the National Key Sci-Tech Special Project of Infectious Diseases (2008ZX10002–022 to YX), and the National Natural Science Foundation of China (30873039 to YX).

Notes

J. Ai, Q. Tang, Y. Wu, and Y. Xu contributed equally to this work. M. Geng and J. Ding designed and supervised this study, analyzed the data, and wrote the article. J. Fan supervised the analysis and comparison of human hepatocellular carcinoma microarray data. J. Ai designed and performed experiments, collected and analyzed data, and cowrote the article. Q. Tang and Y. Wu designed and performed experiments, collected, and analyzed data. Y. Xu analyzed and compared human hepatocellular carcinoma microarray data and cowrote part of the article. Y. Chen helped design and conduct the in vivo lung metastasis experiment. T. Feng, R. Zhou, X. Gao, X. Yue, and Q. Pan technically assisted with experiments and collected and analyzed data. S. Xu performed experiments in initial stages of the project. Q. Zhu contributed to the comparison of human hepatocellular carcinoma microarray data. J. Daugherty-Holtrop, Y. He, and H. E. Xu designed and performed the urokinase-type plasminogen activator assay. J. Li conducted experiments in initial stages of the project, and M. Huang contributed to the discussion of the article and editing the figures.

We thank professors Qiang Yu (Shanghai Institute of Materia Medica, Shanghai, China), Junying Yuan (Harvard Medical School, Boston, MA), Kunliang Guan (University of California, Los Angeles, CA), and Min Li (Johns Hopkins University, Baltimore, MD) for their valuable comments and critical review of the article. We are grateful to the patients and clinicians in Zhong Shan Hospital. We thank Dr Bo Yang and Dr Yuan Ji for assessing immunohistochemical staining of hepatocellular carcinoma tissue microarray. We wish to thank Lijuan Lu, Yong Xi, and Yanyan Shen for providing technical support for the in vivo lung metastasis experiments (Shanghai Institute of Materia Medica). We also wish to thank Dr Finn-Eirik Johansen (Rikshospitalet University Hospital, Oslo, Norway) for providing the pcDNA3.1-pIgR plasmid.

Affiliations of authors: Division of Anti-tumor Pharmacology, State Key Laboratory of Drug Research, Shanghai Institute of Materia Medica, Chinese Academy of Sciences, Shanghai, China (JA, YC, XG, XY, QP, MH, JD, MG); Department of Pharmacology and Glycobiology, School of Medicine and Pharmacy, Ocean University of China, Qingdao, Shandong, China (QT, YW, TF, RZ, SX, JL, MG); Department of Liver Surgery, Liver Cancer Institute, Zhongshan Hospital and Shanghai Medical School, and Institute of Biomedical Sciences, Fudan University, Shanghai, China (YX, QZ, JF); Laboratory of Structural Sciences, Van Andel Research Institute, Grand Rapids, Michigan (JD-H, YH, HEX); Center for Structural Biology of Drug Targets, Shanghai Institute of Materia Medica, Chinese Academy of Sciences, Shanghai, China (HEX).